Systematic identification of cancer cell vulnerabilities to natural killer cell-mediated immune surveillance

Matthew F. Pech, Jacqueline E. Villalta, Leanne J.G. Chan, Samir Kharbanda, Jonathon J. O'Brien, Fiona E. McAllister, Ari J. Firestone, Calvin H. Jan, Jeff Settleman[#]

Calico Life Sciences LLC, 1170 Veterans Boulevard, South San Francisco, CA, United States

[#]correspondence: settleman@calicolabs.com

Abstract

Only a subset of patients respond to therapies that stimulate T-cell responses to cancer, highlighting the need for alternative strategies to promote anti-cancer immunity. Here, we performed genome-scale CRISPR-Cas9 screens in a human MHC-deficient leukemic cancer cell line to systematically identify perturbations that enhance natural killer (NK) effector functions. Our screens defined critical components of the tumor-immune synapse and highlighted the importance of cancer cell interferon-γ (IFNγ) signaling in promoting NK activity. Surprisingly, we found that loss of the cullin4-RING E3 ubiquitin ligase (CRL4) substrate adaptor DCAF15 strongly sensitized cancer cells to NK-mediated clearance. DCAF15 disruption led to an inflamed state in leukemic cancer cells associated with increased expression of the lymphocyte costimulatory molecule CD80, which triggered NK activation. Biochemical analysis revealed that DCAF15 interacts directly with cohesin complex members SMC1 and SMC3. Treatment with indisulam, an anticancer drug reported to function through DCAF15 engagement, was able to phenocopy genetic disruption of DCAF15. In AML patients, reduced DCAF15 expression was associated with improved survival. These findings suggest that inhibition of DCAF15 may have useful immunomodulatory properties in the treatment of myeloid neoplasms.

Introduction

Major advances in tumor control have recently been achieved by targeting immune inhibitory signaling pathways. Treatment with "checkpoint inhibitors," antibodies targeting PD1, PD-L1, or CTLA4, lead to durable responses across a wide range of indications, but only in a subset of patients. Treatment response is positively correlated with tumor mutational burden and infiltration of CD8+ effector T cells, which recognize tumor cells via peptides bound to major histocompatibility complex class I (MHC-I) molecules, suggesting that checkpoint inhibitors work best at clearing highly immunogenic cancers with repressed T cell responses [1-3]. Substantial efforts are being made to extend the benefits of immunotherapy to additional patients. This includes approaches such as combining checkpoint inhibitors with other therapies, drugging additional lymphocyte-suppressive pathways, and boosting the activity of other arms of the immune system [4].

Resistance to therapy has long been a major problem in cancer treatment. Drugs targeting tumor growth processes can profoundly reduce tumor burden, but resistance invariably arises, driven by the substantial genetic and phenotypic heterogeneity present within human tumors [5]. Recent clinical and experimental data have similarly highlighted the ability of cancer cells to escape checkpoint inhibitor-induced immune control. B2M and JAK1/2 mutations have been identified in melanoma patients with acquired resistance to checkpoint inhibitors [6,7]. These mutations impair recognition of the tumor by the adaptive immune system, either by directly disrupting antigen presentation or by rendering the cells insensitive to IFNγ, an important inducer of MHC-I expression. Functional genetic screens using T cell-cancer cell cocultures have highlighted similar mechanisms of resistance *in vitro* [8-11]. Even treatment-naïve tumors can be highly immuno-edited, presenting with IFNγ pathway mutations, reduced MHC-I expression and loss of the peptide sequences that can serve as antigens [12-15]. Together, these findings highlight a critical need for therapies that can either increase MHC expression or work in a MHC-independent fashion.

Anti-tumor immunity is not solely mediated by the adaptive immune compartment. Innate immune cells, most notably natural killer (NK) cells, can have both direct tumoricidal activity and also help to fully elaborate long-lasting anti-tumor responses [16-19]. NK cells are cytotoxic lymphocytes

capable of mounting rapid responses to damaged, infected, or stressed cells, including cancer cells. T and NK cells share effector functions, releasing cytokines and exocytosing lytic granules upon activation to kill target cells. However, NK activation status is controlled by the integrated signals from germline-encoded NK-activating and -inhibiting receptors (aNKRs/iNKRs). Generally speaking, iNKR ligands are expressed by normal and healthy cells, whereas aNKR ligands are upregulated after DNA damage or viral insult [19,20]. MHC-I molecules provide a potent inhibitory signal sensed by NK cells, enabling the innate immune system to respond productively to MHC-deficient cells. As a result, there is considerable interest in amplifying NK responses to cancers, as well as developing NK-based cell therapies [18-20].

Here, we performed genetic screens in an MHC-deficient leukemic cell line to systematically identify modulators of NK-mediated anti-cancer immunity. These screens, unexpectedly, pointed to the potential therapeutic utility of targeting the CRL4 substrate adaptor DCAF15 in myeloid malignancies. Disruption of DCAF15 strongly sensitized cancer cells to NK-mediated killing, resulting from increased cancer cell expression of lymphocyte costimulatory molecules. Proteomic experiments revealed that DCAF15 interacted with the cohesin complex components SMC1 and SMC3. Treatment with indisulam, an anticancer drug that modulates DCAF15 function, reduced interaction with cohesin members and mimicked DCAF15 loss-of-function immunophenotypes.

Results

A genome-scale CRISPR screen identifies modulators of NK effector functions

K562 human chronic myelogenous leukemia cells are a NK-sensitive cancer cell line that weakly expresses MHC-I. To enable a genome-scale CRISPR screen to identify genes that affect the susceptibility of K562 cells to NK-mediated killing in a co-culture assay, we employed NK-92 cells, a human lymphoma-derived cell line phenotypically similar to activated NK cells.[21] These cells exhibit interleukin-2 (IL2)-dependent growth, express a large number of aNKRs and few iNKRs [22], and display potent cytolytic activity against K562 cells. For screening purposes, a clonal isolate of K562 cells expressing high levels of spCas9 was generated and validated (Fig. S1A-C).

91 In pilot experiments, labelled K562 cells were co-cultured with NK-92 cells to determine an
92 effector-to-target (E:T) ratio that applied sufficient selective pressure in the context of a screen
93 (Fig. S1D-F). IL2 was removed during the co-culture to promote the eventual death of NK-92
94 cells, allowing the collection of genomic DNA preparations undiluted by effector cell DNA. A
95 multi-day timeframe between NK challenge and screen readout was used to capture tumor cell
96 fitness changes related both to the direct cytolytic activities of NK cells as well as the longer-term
97 effects from NK-released cytokines.
98
99 For the co-culture screen, cas9-expressing K562 cells were infected with a genome-scale single
100 guide RNA (sgRNA) library targeting all unique coding genes and miRNAs, as well as one
101 thousand non-targeting controls. Seven days post-infection, cells were either grown normally or
102 challenged with NK-92 cells at a 1:1 or 2.5:1 E:T ratio, reducing K562 cell counts 19-fold or 43-
103 fold, respectively, by the end of the screen (Fig. 1A-B). Deep sequencing was used to compare
104 changes in sgRNA abundance between the challenged and unchallenged state after 8 days of co-
105 culture, and genes were ranked using the MAGeCK software [23]. (Fig. 1C, Table S2) There was
106 good agreement between the results from screens performed at the different E:T ratios (Fig. S2A).
107
108 Inspection of the screening results revealed two broad classes of "hits"— sgRNAs targeting
109 components of the tumor-immune synapse or components of the IFNγ signaling pathway (Fig. 1C-
110 D). Disruption of Intercellular Adhesion Molecule 1 (ICAM1) was the top-ranked NK evasion
111 mechanism, scoring many orders of magnitude stronger than any other gene—an observation
112 consistent with the critical role of ICAM1-LFA1 interactions in establishing initial target-
113 lymphocyte adhesion and polarizing cytotoxic granules towards the synapse [16]. Single guide RNAs
114 targeting multiple other tumor-immune synapse components were also enriched after NK
115 challenge, including NCR3LG1 (#26-ranked gene by MaGeCK score), the activating ligand for
116 NKP30 on NK cells [24]; CD58 (#37), an adhesion molecule that binds CD2 [25,26] ; and CD84 (#80),
117 a SLAM-related receptor that binds homotypically to promote activation and cytokine secretion in
118 lymphocytes [27,28]. Other than NECTIN2/PVRL2, sgRNAs targeting NK-inhibitory surface
119 proteins did not score prominently as NK-sensitization mechanisms, consistent with the weak
120 MHC-I expression on K562 cells and the limited repertoire of NK inhibitory receptors expressed

121 on NK-92 cells [22]. NECTIN2 transmits both stimulatory or inhibitory signals to NK cells,
122 depending on whether it is bound to DNAM1 (CD226) or TIGIT, respectively [29,30].
123
124 Besides ICAM1, the top 10 highest scoring NK evasion mechanisms were dominated by sgRNAs
125 targeting the proximal components of the IFNγ signaling pathway, including STAT1, JAK1,
126 IFNGR2, JAK2 and INFGR1 (Fig. 1D). Significantly, IFNγ is not directly cytotoxic or cytostatic
127 to K562 cells (see [31] and Fig. 5), suggesting that the sensitizing effect of the cytokine was
128 downstream of its immunomodulatory effects. Consistent with the important role of IFNγ pathway
129 engagement, sgRNAs targeting negative regulators of the interferon response were strongly
130 depleted after NK challenge. Disruption of the protein tyrosine phosphatases PTPN2 and PTPN1
131 were the #2 and #5 ranked NK-sensitizing mechanisms, respectively. Presumably, these proteins
132 suppress IFNγ-induced immunomodulation by dephosphorylating STAT and JAK proteins, as has
133 been reported in CRISPR screens using T-cell coculture systems or syngeneic tumor models [9,10].
134 Taken together, these findings indicate that our *in vitro* functional genomics screens effectively
135 revealed known components of physiologically-relevant immune synapse and cytokine pathways.
136
137 **Prospective identification of novel genes affecting sensitization to NK cells**
138
139 Mechanisms of NK sensitization identified in the screen were diverse, revealing many strongly-
140 scoring genes not previously linked to either interferon signaling or NK cell biology (Fig. 1E).
141 Most surprisingly, disruption of DCAF15, an uncharacterized substrate adaptor for CRL4
142 ubiquitin E3 ligases, was the top-ranked sensitization mechanism. DCAF15 is a member of the
143 large family of DDB1 and Cul4-associated factors (DCAFs) [32]. CRL4 complexes enable cells to
144 mark proteins for destruction by the proteasome system, thereby contributing to the regulation of
145 intracellular protein homeostasis. As substrate adaptors for CRL4, DCAF proteins provide
146 specificity to the complex, determining which client proteins are ubiquitinated [33]. As with most
147 substrate adaptors, the normal client repertoire of DCAF15 is undefined, and relatively little is
148 known about DCAF15's biological function.
149
150 We also noted that disruption of of two cohesin-related genes, STAG2 and HDAC8, scored as NK
151 sensitization factors (ranked #26 and #19, respectively). Cohesin is a ring-shaped complex

152 involved in chromatin replication, organization and repair, with STAG2 acting as a core complex
153 member and HDAC8 controlling chromatin accessibility [34]. Cohesin dysregulation has cell
154 context-specific consequences, including DNA damage and aneuploidy; in leukemic cells, cohesin
155 mutations are thought to enforce stem cell programs by altering chromatin organization [35].
156
157 **A phenotypic screen based on MHC-I upregulation to identify modulators of the**
158 **IFNγ response**
159
160 The prominent role for IFNγ signaling in the immune response to cancer cells, both clinically and
161 in our screens, prompted us to define more specifically which NK-sensitizing genes are involved
162 in modulating the IFNγ response. MHC-I levels are highly upregulated in K562 cells after IFNγ
163 exposure, increasing 5.9+/-0.98 fold after 24hrs of exposure to IFNγ. This induction was increased
164 to 10.01+/-1.63-fold when PTPN2 was disrupted, whereas no upregulation was detected when
165 STAT1 was disrupted (Fig. 2A-B and S3A-B). We therefore used IFNγ-induced cell surface MHC-
166 I expression as a proxy for the strength of the interferon response. K562 cells transduced with a
167 genome-scale CRISPR library were treated with IFNγ for 24hrs and MHC-I expression was
168 measured by flow cytometry. The brightest 20% and dimmest 20% of cells were sorted, and deep
169 sequencing was used to compare sgRNA abundance between the populations (Fig. 2C, Table S3).
170
171 As expected, cells with impaired MHC-I upregulation were highly enriched for sgRNAs targeting
172 the IFNγ-JAK-STAT pathway (IFNGR1/2, JAK1/2, STAT1, IRF1/2), as well as the antigen
173 processing/presentation machinery (B2M, TAP1/2, TAPBP, PDIA3, HLA-C/B) (Fig. 2D).
174 Conversely, disruption of PTPN2 or STAG2 scored well at inducing an exuberant MHC-I
175 response. Surprisingly, sgRNAs targeting epigenetic factors were highly enriched within the
176 brightest MHC-I expressing cells—most prominently, members of the BCOR complex PCGF1
177 and KDM2B, members of the PRC2 complex EZH2 and SUZ12, as well as factors affecting
178 histone methylation/acetylation status.
179
180 Rank-rank comparisons between the NK and MHC screens were informative in defining a core
181 group of genes that appear to play a role in the IFNγ response in K562 cells (Fig. 2E). Comparing
182 sgRNAs enriched after NK challenge with those causing impaired MHC-I upregulation clearly

183 delineated the known proximal components of the IFNγ signaling pathway (IFNGR1/2, JAK1/2,
184 STAT1), and highlighted several poorly characterized genes such as GSE1, SPPL3 and NR2F2
185 (Fig. 2E).
186
187 Surprisingly, comparing sgRNAs depleted after NK challenge with those causing an exaggerated
188 MHC-I response highlighted the CRL4 substrate adaptor DCAF15 most prominently, alongside
189 the cohesin members STAG2 and HDAC8 (Fig. 2E). As expected, negative feedback regulators
190 of the IFNγ pathway (PTPN1 and PTPN2) were also recovered by this analysis. We focused on
191 understanding the function of DCAF15, given its prominence in both the NK sensitization (#1
192 ranked hit at 2.5 E:T ratio; #12 ranked hit at 1:1 E:T ratio) and MHC upregulation (#13 ranked hit)
193 screens.
194
195 **Disruption of DCAF15 enhances NK effector functions**
196
197 We validated and benchmarked novel NK cell sensitizers using a FACS-based competitive co-
198 culture system that mimicked the conditions of the screen (Fig. 3A). Fluorescently-labelled K562
199 cells expressing control or test sgRNAs were co-cultured in the presence of NK cells, and changes
200 in the relative ratios of cell types were measured by flow cytometry after 48 hours (Fig. 3B-C and
201 S4A-D). Differences in the basal growth rates between genotypes were controlled for by co-
202 culturing the cancer cells in the absence of NK cells. As expected, deletion of the adhesion
203 molecule ICAM1 conferred very strong resistance to NK cells (19.7-fold, N=12). Disabling
204 signaling downstream of IFNγ by deleting STAT1 provided a more modest level of protection
205 (2.45-fold, N=8).
206
207 K562s are very sensitive to NK-mediated killing, thereby yielding a large dynamic range for
208 detection of resistance-promoting factors, while limiting the ability of the assay to detect similarly
209 large increases in sensitization. Nevertheless, we were able to validate that multiple independent
210 sgRNAs targeting DCAF15 promoted sensitization to NK cells (1.6-fold change, N=48). As
211 positive controls, disruption of NECTIN2 or PTPN2 induced a similar degree of sensitization
212 (NECTIN2: 1.95-fold change, N=6; PTPN2: 1.4-fold change, N=12). These findings implicate
213 DCAF15 as a novel modulator of NK-mediated cancer cell immunity.

214

215 **Loss of the cullin-RING E3 ligase substrate adaptor DCAF15 leads to an inflamed state**
216 **distinct from dysregulated IFNγ signaling**

217

218 DCAF15 was a strong hit in both the NK sensitization and MHC upregulation screens, suggesting
219 that DCAF15 disruption sensitizes K562 cells to NK-mediated killing by dysregulating the IFNγ
220 response. Consistent with the screening results, polyclonal cells expressing DCAF15 sgRNAs
221 ("DCAF15 KO cells") displayed 2.45-fold higher levels of MHC-I than control knockout cells
222 after 24hrs of IFNγ exposure, an effect comparable in magnitude to PTPN2 disruption (Fig. 4A).
223 We then tested whether DCAF15 KO cells exhibited hallmarks of dysregulated JAK-STAT
224 signaling, using disruption of PTPN2 as a positive control. We were unable to see any difference
225 in induction of STAT1 phosphorylation after IFNγ exposure in DCAF15 KO cells, or differences
226 in steady state levels of STAT1/2, JAK1/2 or IFNGR1 (Fig. 4B and data not shown). DCAF15 KO
227 cells appeared healthy and proliferated at a normal rate (Fig. S5A). Upon long-term exposure to
228 IFNγ, DCAF15 disruption did not induce a synthetic fitness defect with IFNγ (Fig. 4C). In contrast,
229 PTPN2 KO cells showed higher levels of $STAT1^{PY701}$ induction after IFNγ exposure, and their
230 proliferative rate was temporarily reduced after transient exposure to IFNγ, or more substantially
231 slowed down by continuous treatment with the cytokine (Fig. 4B-C).

232

233 To explore the mechanism by which DCAF15 was contributing to the NK response, RNA-seq was
234 performed on DCAF15 or PTPN2 KO cells basally and after 24hrs of IFNγ exposure. Clustering
235 analysis clearly showed that PTPN2 KO cells were transcriptionally distinct from control or
236 DCAF15 KO cells (Fig. 4D). PTPN2 KO cells clustered differentially along the IFNγ principal
237 component and were enriched for interferon-associated Gene Ontology (GO) terms both before
238 and after cytokine exposure (Fig. S5B-C). In contrast, DCAF15 KO cells did not show substantial
239 differences in their response to IFNγ (Fig. 4D). However, DCAF15 KO cells were enriched for
240 GO terms associated with NK-mediated cytotoxicity, antigen presentation and cell adhesion,
241 consistent with our phenotypic characterization of these cells (Fig. 4E). Together, these findings
242 indicate that while DCAF15 KO K562 cells exhibit a relatively normal response to IFNγ

243 stimulation, they are nonetheless in an inflamed state primed to interact with cytotoxic
244 lymphocytes.
245
246 **Increased NK cell triggering by DCAF15 knockout cells mediated by CD80 expression**
247
248 Intriguingly, differential RNA analysis showed that one of the most highly upregulated genes in
249 DCAF15 KO cells was CD80 (Fig. 4F; Q value 3.7e-23, Beta value 0.98). CD80 is an important
250 co-stimulatory molecule for lymphocytes. CD80 and other B7 family members regulate T cell
251 activation and tolerance by ligation to CD28, CTLA4 or PDL1 [36]. CD80 expression is typically
252 upregulated after the activation of antigen-presenting cells (APCs), providing critical secondary
253 signals to T cells [37]. While mostly studied in the context of T cell biology, B7 family molecules
254 are known to be activating receptors for NK cells, with both CD28-dependent and -independent
255 ways that NK cells receive this signal [38-42].
256
257 K562 cells are an undifferentiated and multipotential CML cell line, well-studied for their ability
258 to differentiate towards many different lineages, including APC-like states [43]. We hypothesized
259 that upregulation of CD80 in DCAF15 KO cells may reflect a broader acquisition of APC-like
260 properties. Immunophenotyping of unstimulated DCAF15 KO cells revealed higher levels of the
261 APC markers CD80, CD40 as well as class I and II MHC molecules (Fig. 5A; 2.23-fold CD80
262 increase; 2.01-fold CD40 increase; 1.44-fold MHC-I increase; 1.22-fold MHC-II increase).
263 DCAF15 KO cells did not display higher levels of the APC maturation marker CD83 (Fig. 5A) or
264 altered expression of various receptors identified in the screen to be important for NK adhesion,
265 activation, or inhibition (Fig. S6A). Importantly, the changes to the DCAF15 KO cell
266 immunophenotype could be rescued by constitutive expression of a sgRNA-resistant DCAF15
267 open-reading frame (Fig. S6B-D).
268
269 Transducing tumors with B7 family members can enhance anti-tumor immunity by enabling the
270 tumor cells to directly deliver antigenic and costimulatory signals to T and NK cells [38,39,44,45]. In
271 our model system, we confirmed that NK-92 cells were competent to receive CD80 stimuli--
272 expressing CD28 but not CTLA4 (Fig. S6E). K562 cells stably over-expressing wild-type CD80
273 were generated (Fig. 5B; 49-fold higher CD80 levels than endogenous). Over-expression was

274 sufficient to increase K562 sensitivity to NK-92 mediated killing (Fig. 5C), whereas
275 overexpression of a mutant form of CD80 carrying point mutations that abrogate CD28 binding [46]
276 ($CD80^{Q65A,M72A}$) had no effect.
277
278 We next determined whether the increased CD80 expression in DCAF15 KO cells was important
279 for their altered NK sensitivity. K562 cells were pretreated with either control or CD80 blocking
280 antibodies prior to exposure to NK-92 cells (Fig. 5D). NK sensitivity was measured by the ability
281 of K562 cells to trigger NK cell degranulation, as measured by NK cell CD107a expression. As
282 expected, ICAM1 KO cells triggered less NK degranulation than control cells (by 52±12%) and
283 were not significantly affected by CD80 antagonism (Fig. 5E). DCAF15 KO cells showed a 17±8%
284 increased ability to trigger NK cells and were approximately twice as sensitive to CD80
285 antagonism compared to control cells (Fig. 5E-F). Following CD80 antagonism, degranulation
286 triggered by DCAF15 KO was not significantly different from untreated control cells. Taken
287 together, these results indicate that DCAF15 disruption in K562 cells induces an APC-like
288 immunophenotype conducive to promoting lymphocyte responses, with higher CD80 expression
289 especially important for increased NK cell triggering.
290
291 **The anti-leukemia drug indisulam inhibits DCAF15 function**
292
293 Aryl sulfonamide drugs have demonstrated promising anti-cancer properties in hematological
294 malignancies [47]. Recently, it was discovered that these agents work via interaction with the CRL4-
295 DCAF15 E3 ubiquitin ligase, promoting its action on the essential splicing factor RBM39 as a
296 neosubstrate [48,49]. This mechanism of action is conceptually similar to that of the "IMiD"
297 thalidomide analogs, which interact with the CRL4-cereblon E3 ubiquitin ligase to promote
298 neosubstrate interactions with various lymphocyte transcription factors [50-52]. Presumably,
299 sulfonamides and IMiDs also impair the degradation of the normal client proteins when they
300 induce neomorphic activity of the substrate adaptor. This has not been proven, however, as it is
301 difficult to systematically determine the normal substrate repertoire of adaptor proteins.
302
303 We hypothesized that treating K562 cells with low concentrations of the aryl sulfonamide
304 indisulam would phenocopy DCAF15 depletion (Fig. 6A). Three-day dose-response experiments

305 revealed that K562 cells were sensitive to indisulam, and that DCAF15 disruption reduced this
306 sensitivity, consistent with previous reports ([49] and Fig. 6B). Dose-response experiments across a
307 panel of 16 hematological cancer cell lines confirmed the reported [48] positive relationship between
308 DCAF15 mRNA expression levels and indisulam sensitivity (Fig. S7A; R^2=0.33, P=0.02).
309
310 We empirically determined that 100nM indisulam treatment lowered RBM39 levels while
311 minimally affecting cell viability and proliferation over a four-day period (Fig. 6C-D and [49]).
312 Remarkably, this treatment regime was able to recapitulate the increased CD80 expression seen in
313 DCAF15 KO cells (Fig. 6E; 2.14-fold increase), and more modestly, the effects on MHC-I and
314 CD40 expression (1.36-fold and 1.27-fold increase, respectively). CD80 upregulation was first
315 detected 24hrs after treatment initiation and plateaued after 48hrs (Fig. S8B). Importantly,
316 indisulam treatment did not further upregulate CD80 in DCAF15 KO cells, suggesting that the
317 drug's effect on CD80 levels was entirely mediated through DCAF15 (Fig. 6F).
318
319 To extend these observations to other cell lines, a panel of hematological cancer cell lines was
320 screened to identify those with detectable CD80 expression (Fig. S7C). The CML cell line KU812
321 expressed similar levels of CD80 as K562, whereas the Daudi lymphoma cell line expressed
322 significantly higher basal CD80 levels. These cells lines were subjected to similar 4-day low-dose
323 regimes of indisulam, which only modestly affected the growth and viability of the cells (Fig.
324 S7D). Remarkably, both Daudi and KU812 cells up-regulated CD80 levels after indisulam
325 treatment, to an extent comparable to that which was observed in K562 cells (Fig. 6G; 2.45-fold
326 for Daudi, 1.71-fold for KU812). Indisulam was not able to induce *de novo* CD80 expression in
327 CD80-negative cell lines (Fig. S7E). Thus, in certain cellular contexts, aryl sulfonamides are
328 immuno-modulatory agents that alter co-stimulatory protein levels by disrupting the normal
329 functions of DCAF15.
330
331 **Reduced DCAF15 expression is associated with improved survival in AML patients**
332
333 Given the *in vitro* findings, we hypothesized that lower DCAF15 expression in myeloid
334 malignancies could be associated with better clinical outcomes. We tested this hypothesis using
335 publicly available acute myeloid leukemia (AML) datasets [53,54]. In both adult and pediatric AML,

336 lower expression of DCAF15 mRNA was associated with increased median overall survival time
337 (Fig. 6H-I). The improved survival of DCAF15-low patients was not driven by a correlation
338 between DCAF15 expression and more aggressive AML subtypes (Fig. S7F-G). Taken together,
339 these findings indicate that lower DCAF15 function, achieved pharmacologically or by genetic
340 means, is associated with favorable immunophenotypes *in vitro* and improved outcomes in AML
341 patients.
342
343 **CRL4-DCAF15 directly interacts with cohesin complex members**
344
345 The normal substrate repertoire of DCAF15 is unknown. To systemically identify direct DCAF15
346 client proteins, we undertook proximity-based proteomic analysis of DCAF15 interaction partners
347 (Fig. 7A). DCAF15 was fused to a promiscuous bacterial biotin ligase [55] ("DCAF15-BioID") and
348 stably expressed in K562 cells, enabling recovery of interaction partners by streptavidin pull-
349 down. In pilot experiments, we confirmed that exogenous C-terminally tagged DCAF15 was able
350 to rescue DCAF15 KO phenotypes and associate with CRL4 complex members DDB1 and
351 CUL4A (Fig. S6B-D, Fig. S8A). During stable DCAF15 overexpression, we observed that the
352 basal concentration of biotin in the media (~3μM) was sufficient to induce BioID activity in the
353 absence of exogenous (50μM) biotin supplementation (Fig. 7B). However, proteasome inhibition
354 by MG132 increased accumulation of DCAF15-BioID and biotinylated species. As a control,
355 results were compared to a GFP-BioID fusion, expected to generically biotinylate proteins. GFP-
356 BioID accumulated much more readily than DCAF15-BioID, and its biotinylation activity was not
357 affected by MG132 treatment.
358
359 After 24hrs of biotin and MG132 treatment, biotinylated protein species were recovered under
360 stringent denaturing conditions. Isobaric labelling and mass spectrometry were used to
361 quantitatively compare the DCAF15 interactome to the GFP interactome (Fig. 7C and Table S5).
362 This approach clearly recovered DCAF15 and the core CRL4 complex, including DDA1, DDB1
363 and CUL4A (DCAF15: 155.6-fold change, P=2.5e-152; DDA1: 24.5-fold change, P=6.5e-139;
364 DDB1: 4.86-fold change, P=8.1e-21; CUL4A: 3.8-fold change, P=8.5e-18).
365

366 Surprisingly, two of the most differentially biotinylated proteins were the cohesin complex
367 members SMC1A and SMC3 (SMC1: 2.39-fold change, P=0.00098; SMC3: 2.76-fold change,
368 P=5e-5). We confirmed the interaction between DCAF15-BioID and endogenous SMC1 and 3 by
369 streptavidin-pulldown followed by western blotting (Fig. 7D). To determine whether this
370 association with cohesin was a generic feature of CRL4 complexes or specific to the CRL4 loaded
371 with DCAF15, we examined the interaction partners of a different substrate adaptor. DCAF16 is
372 a nuclear-localized CUL4 substrate adaptor, which, like DCAF15, interacts with DDB1 despite
373 lacking a canonical WD40 docking domain[32]. When stably expressed in K562 cells, DCAF16-
374 BioID fusions accumulated similarly to DCAF15-BioID, interacted with DDB1 but did not
375 biotinylate SMC proteins (Fig. 7E). As low concentrations of indisulam phenocopy certain aspects
376 of DCAF15 depletion (Fig. 6), we wondered whether indisulam treatment would alter the
377 interaction of DCAF15 with cohesin. DCAF15-BioID cells were treated with indisulam for
378 72hours, with biotin and MG132 added for the final 18hours. This treatment regime lead to
379 substantial indisulam-dependent biotinylation of RBM39 and reduced recovery of biotinylated
380 SMC proteins (Fig. 7E). These findings indicate that cohesin proteins may be *bona fide*
381 ubiquitination substrates for DCAF15, as DCAF15 interacts with SMC proteins in a way that is
382 increased by proteasome inhibition, reduced by indisulam treatment and specific to CRL4-
383 DCAF15.
384
385 **Discussion**
386
387 T cell immunity necessitates antigen recognition in the context of MHC, a requirement unchanged
388 by checkpoint inhibitor therapy. Clinical and experimental data have revealed that disrupting
389 optimal antigen presentation levels is a common mechanism by which cancer cells escape
390 recognition by the adaptive immune system. These findings have highlighted the need for
391 therapeutic strategies that can promote antigen presentation, or that work in a MHC-independent
392 fashion. One such approach involves modulating the NK cell compartment to promote anti-cancer
393 immunity. NK cells integrate the signals from multiple activating and inhibitory receptors to strike
394 the right balance between auto-immunity and sanitization. Here, we discovered that the
395 combinatorial logical of NK activation proved particularly amenable to CRISPR screening,
396 leading to the discovery and validation of a novel factor that enhances NK effector functions when

397 disrupted. The biology was explored within the context of co-cultured NK-92 and K562 cells, a
398 relatively simple model of the interaction between cancer cells and unlicensed NK cells. Despite
399 this limitation, the screens clearly identified known lymphocyte adhesion factors and aNKR
400 ligands, such as ICAM1, NCR3LG1, CD58 and CD84. Other strongly-scoring genes encoding cell
401 surface proteins, such as CEACAM7, IL23R and PTGFRN, may represent novel activating stimuli
402 for NK cells. Extending our genetic screening approach to other types of tumor cells and natural
403 killer subtypes will likely enable a more complete understanding of the relative importance of
404 various aNKRs and iNKRs, and could facilitate the identification of candidate ligands for orphan
405 NK receptors.
406
407 In this screening context, the dominant cytokine signature was clearly associated with IFNγ. There
408 was no evidence of a contribution from TNFα, the other prominent cytokine secreted by NK cells.
409 Unlike other published tumor:cytotoxic lymphocyte co-culture screens [8,10], neither TNFα nor IFNγ
410 was directly cytostatic or cytotoxic to our cancer cell model, likely explaining why components of
411 the immune synapse scored so much more prominently. The importance of IFNγ in our screen
412 reflected the immunomodulatory nature of the cytokine, helping to prime the cancer cells to
413 undergo a productive interaction with lymphocytes. A notable exception was seen with disruption
414 of PTPN2, a negative regulator of IFNγ signaling. Loss of PTPN2 both altered tumor cell
415 immunophenotypes and reduced tumor cell growth after IFNγ treatment. PTPN2 disruption has
416 proven to enhance activated T-cell mediated killing, as well as potentiate the effect of
417 immunotherapy in syngeneic tumor models [9,10,56]. These data suggest that targeting PTPN2 may
418 be a generalizable strategy to sensitize tumor cells to multiple arms of the immune system.
419
420 The importance of the cancer cell IFNγ response in promoting optimal lymphocyte responses
421 prompted us to systemically identify perturbations that augment cytokine-induced MHC-I
422 upregulation. As expected, this screen clearly delineated the proximal components of the IFNγ-
423 JAK-STAT pathway, as well as the antigen processing/presentation machinery. Surprisingly,
424 disruption of a poorly characterized substrate adaptor for the CRL4 E3 ligase was a top scoring hit
425 in both the MHC-I and NK screens. We therefore focused our efforts on understanding the role of
426 DCAF15 function. We determined that DCAF15 KO cells did not have a grossly dysregulated
427 response to IFNγ. Instead, the higher levels of MHC-I following DCAF15 disruption reflected a

428 broader phenotypic change reminiscent of APC activation, with the upregulation of a variety of
429 co-stimulatory and antigen-presenting molecules (Fig. 7F). The upregulation of CD80 in DCAF15
430 KO cells was especially important for increasing NK-92 cell triggering. Given the array of changes
431 elicited by DCAF15 disruption, it will be important to determine how the triggering of primary
432 NK cell populations is altered by DCAF15 KO cells. It is conceivable that unlicensed NK cells,
433 lacking expression of inhibitory self-MHC receptors, may be most responsive to the DCAF15 KO
434 immunophenotype.
435
436 Our data suggest that the surface factors upregulated by DCAF15 disruption are not direct client
437 proteins of the substrate receptor, but rather represent events secondary to altered turnover of the
438 normal DCAF15 client protein(s). We pioneered a novel approach to systemically purify substrates
439 of DCAF family members, as conventional biochemical methods are poorly suited to recover the
440 transient, low-affinity interactions between substrate adaptors and client proteins. The use of
441 DCAF-BioID fusion proteins and proteasome inhibition protects labile substrates from
442 degradation and robustly recovers biotinylated proteins under stringent, denaturing conditions. We
443 anticipate this will be a generalizable strategy for discovering client proteins for the whole family
444 of CUL4 CRL substrate receptors.
445
446 Proteomic analysis and subsequent validation experiments showed that DCAF15-BioID interacted
447 with core CRL4 complex members, and surprisingly, cohesin members SMC1 and SMC3. We
448 were intrigued by this interaction given the similar CRISPR screening scoring pattern of DCAF15
449 to the cohesin factors STAG2 and HDAC8 (Fig. 2E); the shared roles of cohesin and CRL4 E3
450 ligases in DNA metabolism, organization, replication and repair [34,57,58]; and the ability of cohesin
451 mutations to dysregulate hematopoietic differentiation in myeloid malignancies [35]. While not
452 proven here, we hypothesize that SMC1 and SMC3 are direct ubiquitination substrates for
453 DCAF15, given that their interaction was increased on proteasome inhibition, reduced by
454 indisulam treatment, and not seen with unrelated DCAF substrate adaptors. Rather than globally
455 controlling SMC protein levels, we speculate that CRL4-DCAF15 complexes ubiquitinate cohesin
456 at specific genomic sites to regulate chromatin topology or repair (Fig. 7F). In this model,
457 disruption of either STAG2, HDAC8 or DCAF15 impair cohesin function with overlapping
458 phenotypic consequences.

459

460 Recently, it was discovered that aryl sulfonamide drugs including indisulam are capable of binding
461 to DCAF15 and altering CRL-DCAF15 substrate specificity towards the splicing factor RBM39
462 [48,49]. The cytotoxic effects of indisulam were driven by splicing defects resulting from RBM39
463 degradation. Our studies confirmed indisulam-induced RBM39 degradation and the indisulam-
464 dependent interaction between DCAF15 and RBM39. We also discovered indisulam-induced
465 phenotypes attributable to inhibition of DCAF15's normal functions. Concentrations of indisulam
466 with limited RBM39 degradation or cytotoxicity had immunomodulatory properties that
467 phenocopied genetic DCAF15 disruption, and were sufficient to reduce the interaction of DCAF15
468 with SMC1/SMC3, putative endogenous client proteins. We also determined that AML patients
469 with naturally occurring lower levels of DCAF15 had improved overall survival. While these
470 clinical data are preliminary in nature, they provide a rationale for drugging DCAF15 in myeloid
471 neoplasms, achieved through judicious dosing of existing anti-cancer sulfonamides or the
472 development of pure DCAF15 inhibitors.
473

474

475 **FIGURES**

476 **Figure 1. A genome-scale CRISPR screen identifies modulators of NK effector functions**

477 A) Overview of the genome-scale NK CRISPR screening system.

478 B) K562 population doublings (PDs) during the CRISPR screen, as measured by total number
479 of live cells. Note that early timepoints from the co-culture reflect the presence of both
480 K562 and NK-92 cells.

481 C) Analysis of the NK CRISPR screen results. Changes in sgRNA abundance were compared
482 between the 2.5:1 E:T co-culture condition and day 15 dropout cells using the MAGeCK
483 algorithm. The top 10 enriched or depleted genes are shown, as rank-ordered by Mageck
484 score; other manually selected genes are highlighted with their rank indicated. FDR, false
485 discovery rate.

486 D) Overview of high-scoring components of the tumor-immune synapse and IFNγ signaling
487 pathway recovered by the screen. sgRNAs against genes enriched after exposure to NK
488 cells are marked in red, while depleted sgRNAs are marked in green.

489

490 **Supplemental Figure 1.**

491 A) Western blot showing spCas9 expression in clonal isolates of K562 cells infected with a
492 Cas9-expressing lentivirus. Asterisk highlights the clone used for screening purposes.

493 B) Measurement of Cas9 activity using an EGFP disruption assay. Cas9-expressing K562
494 cells were infected at a low MOI with a lentivirus expressing EGFP and a sgRNA targeting
495 EGFP. The percent of cells that lost EGFP expression was measured over time by flow
496 cytometry.

497 C) Measurement of Cas9 activity using sgRNAs targeting mismatch-repair (MMR) complex
498 members. A Cas9-expressing K562 clonal isolate was infected at a low MOI with a
499 lentivirus expressing sgRNAs against core members of the MMR complex. Protein
500 disruption was measured by western blot 10 days after sgRNA infection. Note that certain
501 MMR complex members depend on other binding partners for stability.

502 D) Experimental design for determining selective pressure of different effector:target cell
503 ratios. K562 cells were labelled with carboxyfluorescein succinimidyl ester (CFSE) prior
504 to co-culture with NK-92 cells.

505 E) Effect of increasing effector:target cell ratio on total number of viable target cells over
506 time. During early timepoints, CFSE fluorescence was used to generate target cell counts.
507 At later timepoints, total cell counts accurately reflected target cell counts due to NK-92
508 cell death.
509 F) Representative image of K562:NK-92 co-cultures at 5:1 E:T ratio. NK-92 cells (unlabeled)
510 form aggregate structures enveloping the target cells (green). Scale bar, 250μM.
511
512 **Supplemental Figure 2.**
513 A) Analysis of the NK CRISPR screen results performed at a lower E:T ratio. sgRNA
514 abundance was compared between the 1:1 effector:target ratio co-culture condition and day
515 15 dropout cells using the MAGeCK algorithm. The computed false discovery rate (FDR)
516 is plotted against the -log10 transformation of the MAGeCK score. The top 5 enriched or
517 depleted genes are shown, as rank-ordered by MAGeCK score; other manually selected
518 genes are highlighted with their rank indicated in parentheses.
519
520 **Supplemental Table 1**. Design of genome-scale CRISPR library. sgRNA sequences and
521 coordinates of the intended target locus are provided.
522
523 **Supplemental Table 2**. NK CRISPR screen data. Normalized sgRNA counts and MAGeCK
524 analysis output are provided.
525
526 **Figure 2. A phenotypic screen based on MHC-I upregulation to identify modulators of the**
527 **IFNγ response**
528 A) Flow cytometry measurement of MHC-I expression in K562 cells transduced with the
529 indicated sgRNAs after 24hrs of 10ng/ml IFNγ treatment.
530 B) Fold upregulation of MHC-I expression after IFNγ treatment in K562 cells transduced with
531 the indicated sgRNAs. Mean and standard deviation are shown. *** P value= 0.0002, **
532 P value=0.03, Mann-Whitney test.
533 C) Design of CRISPR screen for IFNγ-induced upregulation of MHC-I expression. SSC, side-
534 scatter.

535 D) Analysis of the MHC-I upregulation CRISPR screen results. The MAGeCK algorithm was
536 used to compare sgRNA abundance between cells in the bottom two and top two deciles
537 of MHC-I expression. The false discovery rate (FDR) is plotted against the -log10
538 transformation of the MAGeCK score. The top 5 to 10 enriched or depleted genes are
539 shown, as rank-ordered by MAGeCK score; other manually selected genes are highlighted
540 with their rank indicated in parentheses.
541 E-F) Comparison of the NK and MHC screening results. Results of each screen were rank-
542 ordered based on their MAGeCK score. Select genes are highlighted.
543
544 **Supplemental Figure 3.**
545 A) Western blot of total STAT1 levels in K562 cells infected with control or STAT1 sgRNAs.
546 B) Western blot of PTPN2 levels in K562 cells infected with control or PTPN2 sgRNAs.
547
548 **Supplemental Table 3**. Raw MHC-I screen data. Normalized protospacer counts and MAGeCK
549 analysis output are included.
550
551 **Figure 3. Disruption of DCAF15 enhances NK effector functions**
552 A) Experimental design of competitive co-culture experiments, with FACS data illustrating a
553 sgRNA that enhances NK-mediated killing.
554 B) Representative results from competitive co-culture experiments performed at a 2.5:1 E:T
555 ratio.
556 C) Competitive co-culture results performed at a 2.5:1 E:T ratio and measured 48-96hrs after
557 challenge with NK-92 cells. Mean and standard deviation are shown. *** P-value <0.0001,
558 Mann-Whitney test.
559
560 **Supplemental Figure 4.**
561 A) Measurement of cell surface NECTIN2 expression by flow cytometry in K562 cells
562 expressing control or NECTIN2 sgRNAs. Gates show background levels of fluorescence.
563 B) Measurement of cell surface ICAM1 expression by flow cytometry in K562 cells
564 expressing control or ICAM1 sgRNAs. Gates show background levels of fluorescence.

565 C) Measurement of DCAF15 mRNA expression by RNAseq in K562 cells transduced with
566 control or DCAF15 sgRNAs.
567
568 **Figure 4. DCAF15 disruption leads to an inflamed state distinct from dysregulated IFNγ-**
569 **JAK-STAT signaling**
570 A) Flow cytometry measurement of cell surface MHC-I expression in K562 cells transduced
571 with the indicated sgRNAs after 24hrs of 10ng/ml IFNγ treatment. *** P <0.0001; ** P=
572 0.0044, Mann-Whitney test.
573 B) Western blots against total and phosphorylated STAT1 after 30 minutes of 1ng/ml IFNγ
574 treatment in K562 cells infected with the indicated sgRNAs.
575 C) Growth rate of K562 cells expressing the indicated sgRNAs, cultured normally
576 ("untreated"), treated 24hrs with 10ng/ml IFNγ ("IFNγ pulse"), or retreated with 10ng/ml
577 IFNγ every day ("IFNγ constant").
578 D) Principle component analysis (for principle components (PC) 1 and 3) of transcriptomes
579 from K562 cells expressing the indicated sgRNAs and treated +/- 10ng/ml IFNγ for 24hrs.
580 E) Selected GO terms, identified by RNA-seq, enriched in DCAF15 KO cells. Negative log10
581 transformation of the Benjamini-Hochberg corrected P value.
582 F) Volcano plot of genes differentially expressed between DCAF15 KO cells compared to
583 control KO cells. Selected genes are highlighted. The FDR-corrected P-value generated
584 from a likelihood ratio test (Q-value) is plotted against an approximate measure of the fold
585 change in expression (Beta value).
586
587 **Supplemental Figure 5.**
588 A) Growth rate of K562 cells expressing sgRNAs against DCAF15 or a control gene. Results
589 from 2-3 independent experiments and 2-3 different sgRNAs per gene. Mean and standard
590 deviation are shown. DCAF15 sgRNAs, 1.1+/-0.01 population doublings per day. Control
591 sgRNAs, 1.13+/-0.03 population doublings per day.
592 B) Gene set enrichment analysis (GSEA) of genes differentially upregulated in PTPN2 KO
593 cells. nES, normalized enrichment score. Categories with a FDR Q-value of <0.1 are
594 shaded in blue.
595 C) GSEA of genes differentially upregulated in PTPN2 KO cells after IFNγ treatment.

596

597 **Supplemental Table 4**. List of differentially expressed genes determined by RNA-seq of control,
598 DCAF15 or PTPN2 KO K562 cells.

599

600 **Figure 5. Increased NK triggering by DCAF15 knockout cells mediated by CD80 expression**

601 A) Flow cytometry measurements of the indicated cell surface markers in K562 cells
602 expressing the indicated sgRNAs. N=9-24 samples per condition. *** P<0.0001, **
603 P=0.001, ns P>0.1, Mann-Whitney Test.

604 B) Flow cytometry measurement of CD80 surface expression in control K562 cells or those
605 lentivirally over-expressing CD80. Gate shows level of background fluorescence in
606 unstained cells.

607 C) Competitive co-culture results between indicated K562 cell types and NK-92 cells,
608 performed at 1:1 E:T ratio. * P=0.005, ** P=0.0007, NS P>0.1, unpaired T test. $CD80^{mut}$
609 refers to $CD80^{Q65A,M72A}$ mutant.

610 D) Experimental design of CD80 blockade experiment.

611 E) Effect of blocking antibodies to CD80 on NK-92 activation, measured by CD107 flow
612 cytometry on NK-92 cells after 4hrs of co-culture. Data points from experiments performed
613 on the same day are joined by lines of the same color. ** P=0.03, * P=0.06, ns P>0.1,
614 Wilcoxon matched-pairs signed rank test. Experiment performed 4 times, 2x sgRNAs per
615 condition.

616 F) Percent decrease in NK-92 degranulation after CD80 antibody treatment of indicated target
617 cells. Data points from experiments performed same day are joined by lines. Mean is
618 indicated. ** P=0.03, Wilcoxon matched-pairs signed rank test.

619

620 **Supplemental Figure 6.**

621 A) Flow cytometry measurements of the indicated cell surface markers in K562 cells
622 expressing the indicated sgRNAs. N=2-14 samples per condition. Ns P>0.1, * P=0.04, **
623 P=0.01, Mann-Whitney Test.

624 B) Experimental design for rescuing DCAF15 disruption in K562 by lentiviral expression of
625 a sgRNA-resistant DCAF15 open reading frame.

626 C) Western blot of DCAF15 rescue construct expression.

627 D) Flow cytometry measurements of the indicated cell surface markers in K562 cells
628 expressing the indicated sgRNAs and rescue constructs. N=6-24 samples per condition.
629 *** P<0.0001, ** P=0.004, Mann-Whitney test.
630 E) Flow cytometry measurement of CTLA4 and CD28 expression on NK-92 cells. Gates show
631 background fluorescence levels in unstained cells.
632
633 **Figure 6. The anti-leukemia drug indisulam inhibits DCAF15 function**
634 A) Proposed model for DCAF15 gain- and loss-of-function phenotypes triggered by indisulam
635 treatment.
636 B) Dose response of K562 cells expressing the indicated sgRNAs to indisulam. Relative
637 viability measured by ATP content. N=2 experiments. Mean and standard deviation are
638 shown.
639 C) Growth of K562 cells treated with 0.1μM indisulam over 4 days. N=12 per timepoint.
640 Mean and standard deviation are shown.
641 D) Western blot for total RBM39 levels in K562 cells after 0.1μM indisulam treatment for the
642 indicated number of days.
643 E) Flow cytometry measurements of the indicated cell surface markers in K562 cells after
644 indisulam treatment. Mean and standard deviation are shown. *** P<0.0001, ** P=0.0085,
645 * P=0.013, mean significantly different from 1, one sample T test.
646 F) CD80 expression measured by flow cytometry in indisulam-treated K562 cells expressing
647 the indicated sgRNAs. Mean and standard deviation are shown. N=4-6 samples. **
648 P=0.0095, * P=0.0286, ns P>0.1, Mann-Whitney test.
649 G) Effect of indisulam treatment on CD80 expression in the indicated cell lines. N=3-12
650 samples. Mean and standard deviation are shown. *** P<0.0001, ** P= 0.0066, mean
651 significantly different from 1, one sample T test.
652 H) Kaplan-Meier analysis of overall survival in adult AML patients from TCGA LAML
653 project stratified by DCAF15 expression. “DCAF15 high” and “DCAF15 low” represents
654 patients in top or bottom 50% of DCAF15 expression, respectively. N=142 patients. 95%
655 confidence interval shown. Median survival, 16.17 vs 12.18 months. P-value from log-rank
656 test.

657 I) Kaplan-Meier analysis of overall survival in pediatric AML patients from TARGET project
658 stratified by DCAF15 expression. "DCAF15 high" and "DCAF15 low" represents patients
659 in top or bottom 20% of DCAF15 expression, respectively. N=76 patients. 95% confidence
660 interval shown. Median survival, 21.17 vs NA. P-value from log-rank test.
661
662 **Supplemental Figure 7.**
663 A) Relationship between DCAF15 mRNA expression and indisulam sensitivity across a panel
664 of cell lines.
665 B) Time-course of CD80 expression after indisulam treatment in K562 cells measured by flow
666 cytometry. Blue shading indicates period of CD80 upregulation. N=2-4 samples per
667 timepoint. Mean and standard deviation are shown.
668 C) CD80 expression measured by flow cytometry across a panel of cancer cell lines. Dashed
669 line indicates background level of antibody staining, with cell lines in red have expressing
670 above background levels of the protein. CML, chronic myelogenous leukemia. BL,
671 Burkitt's lymphoma. AML, acute myeloid leukemia. AMoL, acute monocytic leukemia.
672 T-ALL, T-acute lymphoblastic leukemia. MM, multiple myeloma. ALCL, anaplastic large
673 cell lymphoma.
674 D) Growth of Daudi and KU812 cells treated with 0.1μM indisulam over 4 days. N=3 per
675 timepoint. Mean and standard deviation are shown.
676 E) Fold change in CD80 expression in the indicated cell lines after 4 days treatment with
677 0.1μM indisulam.
678 F) Box and whisker plot of DCAF15 expression in TCGA LAML samples, stratified by
679 subtype using the French American British (FAB) AML classification scheme. Analysis
680 from UALCAN portal [59]. Subtypes with significantly different median expression values
681 are indicated.
682 G) FAB classification of adult AML patients in the TCGA LAML project, stratified by top
683 50% ("DCAF15 high") or bottom 50% ("DCAF15 low") of DCAF15 expression.
684
685 **Figure 7. CRL4-DCAF15 directly interacts with cohesin complex members**
686 A) Experimental system for discovering DCAF15 interaction partners by proximity ligation.

687 B) Indicated constructs were stabled expressed in K562 cells, and biotinylated proteins
688 detected by HRP-conjugated streptavidin ("α-biotin"). Asterisks denote major
689 endogenous biotin-containing proteins. "MG132" and "Biotin" refer to 18hrs treatment
690 with 5μM MG132 or 50μM biotin.
691 C) Proteins identified by quantitative mass spectrometry as differentially biotinylated by
692 DCAF15-BioID as compared to GFP-BioID. Log2-fold changes are plotted against
693 precision of the measurement (1/ coefficient of variation). Colors denote the posterior
694 probability that a protein fold change was small (referred to as "P-null" in the legend), as
695 explained in the methods.
696 D-E) Affinity capture of biotinylated proteins by streptavidin beads ("biotin IP") and detection
697 by western blot. Indicates constructs were stably expressed in K562 cells. "Indisulam"
698 refers to 48hrs 0.1μM indisulam treatment prior to MG132 and biotin addition.
699 F) Model of proposed DCAF15 function.
700
701 **Supplemental figure 8.**
702 A) Exogenous DCAF15 interacts with CRL4 core complex members. Indicated constructs
703 were stably expressed in K562 cells. Anti-Flag immunoprecipitations were performed and
704 analyzed by western blot.
705
706 **Supplemental Table 5.** Comparison of biotinylated proteins recovered from K562 cells
707 expressing DCAF15-BIoID or GFP-BioID using isobaric labelling and mass spectrometry.
708
709 **Supplemental Table 6.** List of sgRNA sequences used.
710
711 **Supplemental Table 7.** List of antibodies used.
712
713 **Supplemental Table 8.** Primer design for sequencing sgRNA libraries.
714

715

716 **Materials and methods**

717

718 ***Cell lines***

719 All cell lines were purchased from ATCC and were tested monthly for mycoplasma contamination.
720 Cell lines other than NK-92 were maintained in RPMI supplemented with 10% FBS, 1mM
721 GlutaMAX and 1% antibiotic, antimycotic. NK-92 cells were grown in Myelocult H5100 (Stem
722 cell Technologies) supplemented with 100U/ml human IL-2 (Peprotech cat#200-02). IL-2 stock
723 solution was made by reconstituting lyophilized cytokine to 10e6 U/ml in 50mM acetic acid, 0.1%
724 BSA in PBS.

725

726 ***Construction of the CRISPR Library***

727 CRISPR screening was performed using bespoke genome-scale libraries, to be described in detail
728 elsewhere. In brief, the sgRNA library was designed with 120,021 sgRNAs present, representing
729 6 guides each against 21,598 genes and 4 guides each against 1,918 miRNAs, as well as 1000 non-
730 targeting negative control guides (Table S1). sgRNAs targeting protein-coding genes were based
731 on the Avana libraries [60]. sgRNAs targeting miRNAs were based on the design of the Gecko v2.0
732 libraries [61]. The protospacer library was synthesized by Twist Biosciences. The synthesized oligo
733 library was amplified using emulsion PCR followed by purification. The vaccinia virus DNA
734 polymerase was used to clone the protospacers into a lentiviral construct (In-fusion, Takara). The
735 lentiviral construct was linearized by Bfua1 digestion (New England Biolabs). To ensure complete
736 digestion, Bfua1 activity was stimulated by addition of 500nM of a double-stranded oligo
737 containing a Bfua1 site (5' atagcacctgctata 3') (based on [62]).

738

739 The guide RNAs were expressed from a human U6 promoter, using a modified sgRNA design (A-
740 U flip, longer stem-loop) previously described [63]. An EF1a-Puro-T2A-cerulean-wpre ORF was
741 used for selection purposes and for measuring infection rates. The library was electroporated into
742 MegaX cells and plated across 37x 500cm^2 LB-carbenicillin plates. The library was recovered and
743 pooled by scraping and column-based plasmid purification (Zymopure GigaPrep).

744

745 ***Preparation of virions***

746 16M 293T cells were plated onto 177cm^2 dishes (9x plates total). 24hrs later, cell media was
747 replaced with 32mls of DMEM+10% FBS (D-10). Cells were transfected with the library by
748 lipofection (per plate: 158ul lipofectamine 2000, 8mls of Optimem, 3.95μg of VSVG, 11.8μg of
749 Pax2, 15.78μg of library). The transfection mixture was left on the cells overnight, then changed
750 to 25mls of D-10. Viral supernatant was collected 48hrs later. Debris was removed by
751 centrifugation at 200g. Aliquots were flash-frozen and stored at -80°C.
752
753 ***Validation of the Cas9-expressing cell line used for screening***
754 K562 cells were lentivirally infected with a EF1a-spCas9-T2A-blastR construct. Following
755 10μg/ml blasticidin selection, cells were dilution cloned. Clonal isolates with high levels of cas9
756 expression (as determined by western blot) were selected for further characterization. To determine
757 the kinetics and efficacy of gene cutting under screening conditions (*e.g.*, low MOI of the sgRNA
758 construct), cells were infected with a lentiviral construct expressing both EGFP and a sgRNA
759 targeting GFP. Following puromycin selection, the loss of EGFP expression was monitored by
760 flow cytometry. In other experiments, the ability to effectively deplete endogenous proteins was
761 determined by using a series of sgRNAs targeting the mismatch repair complex and measuring
762 protein depletion by western blot.
763
764 ***The NK cell screen***
765 Five hundred million spCas9-expressing K562 cells were mixed with CRISPR sgRNA library
766 virions and 1L of media, then distributed across 34 6-well plates. Cells were spin-fected at 1900
767 rpm for 30 min at room-temperature with CRISPR library virus, conditions calculated to achieve
768 a MOI of ~0.3 and 1000 cells per sgRNA library representation. MOI was measured by tracking
769 the percent of the population expressing the cerulean marker found in the sgRNA library. Cells
770 were incubated overnight in viral supernatant prior to being pooled, spun down to remove virions,
771 and returned to spinner-flask culture (Bell-Flo Flask, Bellco Glass Inc). 24 to 48hrs post-infection,
772 2μg/ml puromycin selection was started for four days. Cells were maintained in log-growth phase
773 with a minimal representation of 500M cells. Seven days post guide-infection, NK cell challenge
774 was initiated. For the 2.5:1 E:T challenge, 100M K562 cells were mixed with 250M NK-92 cells
775 in 1L of Myelocult, and split across 25 177cm^2 dishes. For the 1:1 E:T challenge, 100M K562 cells
776 were mixed with 100M NK-92 cells in 400mls of Myelocult, and split across 10 177cm^2 dishes.

777 As a control, K562 cells were continuously propagated in RPMI media. 2 days after initiating the
778 NK-92 challenge, the co-culture was switched to RPMI media. NK-92 cells, when grown in RPMI
779 without IL-2, are rapidly lost from the culture. Six days after the media switch, 100M cell pellets
780 were generated for library construction. All cell pellets were stored cryopreserved in cell-freezing
781 media (Gibco #12648).
782
783 ***The MHC-based screen***
784 Generation of K562 cells expressing the sgRNA library was performed as described above. On
785 day 8 post-guide infection, 150M cells were stimulated with 10ng/ml IFNγ (R&D Systems 285-
786 IF). 24hrs later, cells were spun down, washed, and stained in 3mls of 1:200 anti-HLA ABC-APC
787 (W6/32 clone, BioLegend) in PBS, 2% FBS for 30min at 4°c. Approximately 10M of the brightest
788 20% and dimmest 20% of cells were sorted (BD FACSAria Fusion). Cell purity was determined
789 to be >95% by re-analysis post-sorting. A replicate of this experiment was performed on day 14
790 post-guide infection.
791
792 ***CRISPR library preparation and sequencing***
793 Genomic DNA was prepared by thawing cryopreserved cell pellets and proceeding with DNA
794 extraction using column-based purification methods (NucleoSpin Blood XL, Machery-Nagel).
795 Protospacer libraries were generated by a two-step PCR strategy, modified from [64]. In the first
796 round of PCR, 150µg of gDNA (equivalent to 15M K562 cells and 125-fold coverage of the
797 library) was used in a 7.5ml PCR reaction to amplify the protospacers. This reaction was performed
798 using a 500nM mixture of primers containing 0-9bp staggers, to ensure base-pair diversity during
799 Illumina sequencing (see supplemental table S7). The reaction was performed with Phusion master
800 mix (New England Biolabs) and 3% DMSO with the following cycling conditions: 1 cycle X 30 s
801 at 98°C, 21 cycles X 15 s at 98°C, 20 s at 63°C, 15 s at 72°C, 1 cycle X 2 min at 72°C. In the
802 second round of PCR, 4ul of the initial PCR product was used as the template in a 200ul PCR
803 reaction to make the sample compatible with Illumina chemistry and to add unique I5 and I7
804 barcodes to the sample. The reaction was performed with Phusion master mix (New England
805 Biolabs), 500nM primers and 3% DMSO with the following cycling conditions: 1 cycle X 30 sec
806 at 98°C, 12 cycles X 15 s 98°C, 20 s at 60°C, 15 s at 72°C, 1 cycle X 2 min at 72°C. The library
807 was size-selected first by a 1:1 SPRI bead selection (AMPure XP beads, Beckman Coulter),

808 quantified by high-sensitivity dsDNA Qubit (ThermoFisher Scientific), and pooled. An agarose
809 size selection step (PippinHT, Sage Science) was performed prior to sequencing on an Illumina
810 Hiseq4000.
811
812 ***Screen analysis***
813 Libraries were sequenced to a depth of ~20 million reads per condition. Reads were aligned to the
814 sgRNA library using bowtie2. Protospacer count tables were generated from these alignments with
815 python scripts and processed with MAGeCK. MAGeCK analysis was used to score and prioritize
816 sgRNAs, using default settings in the algorithm [23]. A subset of genes, mostly from highly related
817 gene families, have more than 6 sgRNAs targeting them. As the MAGeCK scoring method tends
818 to prioritize consistency of effect over magnitude of effect, genes with more than 6 guides targeting
819 them were excluded from the analysis. MAGeCK scores were -log10 normalized, and values were
820 plotted against FDR values.
821
822 ***Competitive co-culture experiments***
823 Cell were transduced at a high MOI with a lentiviral sgRNA construct expressing the guide of
824 interest, puromycin resistance and CMV promoter-driven expression of a red or green fluorescent
825 protein. Knockout cell populations were maintained in a polyclonal state. Gene disruption was
826 confirmed at the protein level by flow cytometry or western blot, and by RNA-seq when antibody
827 reagents were not available. Complete knockout in >90% of the population was routinely achieved
828 (Fig. S4A-D). Cells were counted and 0.25M red-labelled test cells were mixed with 0.25M green-
829 labelled control cells (expressing a sgRNA against an olfactory receptor gene). The mixture was
830 either grown in RPMI or mixed with 1.25M NK-92 cells in 4mls Myelocult media. The ratio of
831 red-to-green cells was measured 2 to 4 days post-challenge, with the fold-change normalized to
832 the ratio in the non-challenged state (to control for differences in basal cell growth rate).
833
834 ***Flow cytometry***
835 0.5 to 1M cells were spun down and stained with APC-conjugated antibodies for 30mins at 4°c in
836 PBS with 2% FBS. Cells were analyzed on a BD LSRFortessa. The geometric mean fluorescence
837 intensity of singlet, DAPI-excluding cells was measured, and normalized to the background
838 fluorescence of that particular genotype of cells.

839

840 ***DCAF15 rescue experiments***

841 The DCAF15 open reading frame was synthesized based off reference sequence NM_138353, but
842 with silent mutations designed to confer resistance to all three sgRNAs. To ensure resistance to
843 sgRNA-directed gene cutting, silent mutations were introduced to the PAM domain and the
844 proximal region of the protospacer (guide #1: 5' GCTGCACACCAAGTACCAGGTGG to
845 GCTGCACACCAAaTAtCAaGTaG. Guide #2: 5' TGACATCTACGTCAGCACCGTGG to
846 TGACATCTACGTCtcCACaGTaG; Guide #3: 3' GCAGCTTCCGGAAGAGGCGAGGG to
847 GCAGCTTCCGGAAtaaaCGtGGt).

848

849 The rescue construct was expressed lentivirally from an EF1a promoter, with a c-terminal 3-flag
850 epitope tag. Rescue cells were selected with hygromycin. The rescue construct was introduced two
851 weeks after the initial introduction of the DCAF15 sgRNAs, and stable cell lines generated by a
852 week of selection in 375μg/ml hygromycin. Expression of the construct was confirmed by lysing
853 cells in PBS+0.1% NP40 (as per [48]) and western blotting for the Flag tag.

854

855 ***CD80 blocking experiments***

856 RFP-labelled target cells (0, 0.75M, or 2.5M) were resuspended in 0.5mls Myelocult + 5μg/ml
857 control (MOPC-21 clone) or blocking CD80 (2D10 clone) antibodies. Cells were incubated for 30
858 mins at room temperature. 0.5M NK-92 cells in 0.5mls Myelocult were added to the well, as well
859 as 1:200 anti-CD107a-APC antibody. Cells were co-cultured for 4hrs at 37°C. Flow cytometry
860 was used to measured CD107A-APC expression in the NK-92 (RFP-negative) population. NK-92
861 cells were found to display a basal level of CD107a expression in the absence of effector cells.
862 Increases above basal staining levels were used to define NK-92 degranulation. The experiment
863 was repeated 4 times to establish biological replicates.

864

865 ***CD80 over-expression experiments***

866 A full-length CD80 open reading frame, based on reference sequence NM_005191.4, was
867 synthesized with a c-terminal 3x Flag tag and expressed lentivirally from the EF1a promoter. Over-
868 expressing cells were selected with hygromycin. As a control construct, a mutant version of CD80
869 was synthesized with Q65A and M72A mutations in the "V-type" Ig-like domain. Each of these

870 residues makes contacts with CTLA4 in published CD80-CTLA4 co-crystal structures [65] and
871 alanine scanning experiments have shown that these residues are required for CD80 binding to
872 CD28 or CTLA4 [46].
873
874 ***sgRNA sequences used***
875 See supplemental table 6.
876
877 ***Antibodies used***
878 See supplemental table 8.
879
880 ***Cell viability after in vitro cytokine stimulation***
881 Cells were plated at 0.25M/ml in media with or without 10ng/ml IFNγ. Every day, an aliquot of
882 cells was counted (Vi-CELL XR, Beckman Coulter), and cells were diluted in fresh media to
883 maintain them in logarithmic growth phase. Continuously-treated cells were re-fed with fresh
884 10ng/ml IFNγ every day, whereas pulse-treated cells only received 24hrs of cytokine treatment.
885
886 ***Western Blotting***
887 Cells were counted, spun down and washed in PBS prior to lysis in NP40 lysis buffer (25mM
888 HEPES pH 7.5, 150mM NaCl, 1.5mM $MgCl_2$, 0.5% NP40, 10% glycerol, 2mM DTT) with
889 protease and phosphatase inhibitors. Lysates were normalized by cell count and/or protein
890 concentration. 20-40μg of lysates were used for western blot analysis using standard procedures.
891 Antibody binding was detected by enhanced chemiluminescence (SuperSignal Dura, Thermo
892 Scientific).
893
894 ***RNA-sequencing analysis***
895 Cells were seeded at 0.33M/ml density. Twenty-four hours later, 2M cells were collected. RNA
896 was first purified by TRizol extraction and then further purified using column-based methods and
897 polyA selection. RNAseq libraries were constructed using TruSeq Stranded mRNA Library Prep
898 Kits (Illumina) and were sequenced on an Illumina Hiseq4000 machine using 150bp paired-end
899 reads. Transcript abundances were quantified using Salmon[66], with differential expression
900 analysis performed by Sleuth [67].

901

902 ***Indisulam treatment***

903 Indisulam (Sigma SML1225) was reconstituted at 10mM in DMSO and stored in single use
904 aliquots at -80°C. For indisulam dose-response experiments, 5000 cells were plated in 384-well
905 plates (Greiner) and treated with indisulam over a 72hr period. A 12-point dose-response was
906 performed between 10μM and 4.9μM of drug, as dispensed by a Tecan D300e. Cell viability was
907 measured by ATP quantification (Cell Titer Glo, Promega). Dose-response measurements were
908 fitted to a sigmoidal curve and an IC50 determined (Prism, GraphPad Software). DCAF15
909 expression data from different cell lines was downloaded from the Cancer Cell Line Encyclopedia
910 [68] (https://portals.broadinstitute.org/ccle)

911

912 For low-dose indisulam experiments, cells were plated at 0.4M/ml in media with or without 100nM
913 indisulam (1:100,000 dilution of stock). Cells were diluted every day in fresh media and drug to
914 maintain them in logarithmic growth phase. Cells were analyzed for CD80 expression 96 hours
915 after initiation of treatment.

916

917 ***AML survival analysis***

918 FPKM RNAseq quantification for patient samples form the TARGET and TCGA LAML cohorts
919 was obtained from the NIH NCI Genomic Data Commons DATA portal
920 (https://portal.gdc.cancer.gov/) . Clinical data for that TARGET AML and TCGA LAML cohorts
921 were obtained from the Genomic Data Commons DATA portal and the Broad Institute TCGA
922 Genome Data Analysis Center (http://gdac.broadinstitute.org/) respectively. Patients with
923 matching clinical and transcript abundance data patients were stratified by DCAF15 expression as
924 indicated. Survival time and vital status were defined as 'Overall Survival Time in Days' and 'Vital
925 Status' respectively for the Target AML cohort. For the TCGA LAML study survival time for
926 deceased patients ('patient.vital_status'=dead) was defined as 'patient.days_to_death' while for
927 living patients ('patient.vital_status'=alive) 'patient.days_to_last_followup' was used for survival
928 time. Survival analysis and Kaplan–Meier plots were generated using lifelines software for python
929 (https://doi.org/10.5281/zenodo.2584900).

930

931 ***DCAF15 proximity ligation***

932 K562 cells were infected with lentivirus expressing DCAF15-3flag-BioID-HA-T2A-BlastR,
933 DCAF16-3flag-BioID-HA-T2A-BlastR, or 3flag-GFP-T2A-BioID-HA-T2A-BlastR. Stable cell
934 lines were generated by 10µg/ml blasticidin selection. In triplicate, 20M cells were grown in media
935 supplemented with 50µm biotin and 5µm MG132. 18hrs later, cell pellets were washed three times
936 with ice cold PBS and lysed in mild lysis buffer (PBS 0.1% NP40 + PI/PPI), conditions determined
937 to maximize the solubility of over-expressed DCAF15. 1mg of clarified lysate was used for
938 enrichment of biotinylated species. Lysates were mixed with 60ul of streptavidin beads (Pierce
939 #88817) for 4hrs at 4c in 500µl total volume. Beads were collected on a magnetic column, washed
940 twice with 1ml RIPA buffer (25mM HEPES-KOH pH 7.4, 150mM NaCl, 1% Triton X-100, 0.5%
941 sodium deoxycholate, 0.1% SDS, 1mM EDTA) and three times with 1ml urea buffer (2M urea,
942 10mM TRIS-HCl- pH 8.0).
943
944 For western blotting experiments, after urea washing, beads were equilibrated in mild lysis buffer.
945 Elution was performed by incubating the beads 15min at 23°C, 15min at 95°C in 30µl 2.5X
946 Laemlli buffer supplemented with 10mM Biotin and 20mM DTT. The eluate was brought down
947 to 1X concentration with lysis buffer prior to western blotting. We note that detection of total
948 biotinylated species by western blot was extremely sensitive to detection conditions. Membranes
949 were blocked for 10min in PBS, 2.5%BSA, 0.4% Triton-X 100. 1ng/ml streptavidin-HRP in
950 blocking buffer was added for 25min at room temperature. The membrane was washed for
951 15minutes in PBS 0.4% TritonX-100 prior to ECL exposure.
952
953 To measure BioID activity after indisulam treatment, cells were treated for 48hours with 0.1µm
954 indisulam, followed by 24hrs in indisulam with 50µm biotin and 5µm MG132.
955
956 ***Proteomic analysis of DCAF15 interaction partners***
957 For proteomics experiments, after the urea buffer washes, the samples were resuspended in
958 denaturing buffer (8M urea, 50 mM ammonium bicarbonate pH 7.8). Proteins were reduced with
959 dithiothreitol (5 mM, RT, 30min) and alkylated with iodoacetamide (15 mM RT, 45 min in the
960 dark). Excess iodoacetamide was quenched with dithiothreitol (5 mM, room temperature, 20 min
961 in the dark). The samples were diluted to 1 M urea using 50 mM ammonium bicarbonate and then
962 digested with trypsin (37°C, 16h). After protein digestion, samples were acidified with

963 trifluoroacetic acid to a final concentration of 0.5% and desalted using C18 StageTips [69]. Peptides
964 were eluted with 40% acetonitrile/5% formic acid then 80% acetonitrile/5% formic acid and dried
965 overnight under vacuum at 25°C (Labconco CentriVap Benchtop Vacuum Concentrator, Kansas
966 City, Mo).
967
968 For tandem mass tag (TMT) labelling, dried peptides were resuspended in 50µL 200mM
969 HEPES/30% anhydrous acetonitrile. TMT reagents (5 mg) were dissolved in anhydrous
970 acetonitrile (250µL) of which 10µL was added to peptides to achieve a final acetonitrile
971 concentration of approximately 30% (v/v). Following incubation at room temperature for 1 h, the
972 reaction was quenched with 5% hydroxylamine/200mM HEPES to a final concentration of 0.3%
973 (v/v). The TMT labelled peptides were acidified with 50µL 1% trifluoroacetic acid and pooled
974 prior to desalting with SepPak (Waters) and dried under vacuum.
975
976 The pooled TMT-labeled peptides were fractionated using high pH RP-HPLC. The samples were
977 resuspended in 5% formic acid/5% acetonitrile and fractionated over a ZORBAX extended C18
978 column (Agilent, 5µm particles, 4.6 mm ID and 250 mm in length). Peptides were separated on a
979 75-min linear gradient from 5% to 35% acetonitrile in 10mM ammonium bicarbonate at a flow
980 rate of 0.5mL/min on an Agilent 1260 Infinity pump equipped with a degasser and a diode array
981 detector (set at 214, 220, and 254nm wavelength) from Agilent Technologies (Waldbronn,
982 Germany). The samples were fractionated into a total of 96 fractions and then consolidated into 12
983 as described previously [70]. Samples were dried down under vacuum and reconstituted in 4%
984 acetonitrile/5% formic acid for LC-MS/MS processing.
985
986 Peptides were analyzed on an Orbitrap Fusion Lumos mass spectrometer (Thermo Fisher
987 Scientific) coupled to an Easy-nLC (Thermo Fisher Scientific). Peptides were separated on a
988 microcapillary column (100 µm internal diameter, 25 cm long, filled using Maccel C18 AQ resin,
989 1.8µm, 120A; Sepax Technologies). The total LC-MS run length for each sample was 180 min
990 comprising a 165 min gradient from 6 to 30% acetonitrile in 0.125% formic acid. The flow rate
991 was 300 nL/min and the column was heated to 60°C.
992

993 Data-dependent acquisition (DDA) mode was used for mass spectrometry data collection. A high
994 resolution MS1 scan in the Orbitrap (m/z range 500-1,200, 60k resolution, AGC 5 x 10^5, max
995 injection time 100 ms, RF for S-lens 30) was collected from which the top 10 precursors were
996 selected for MS2 analysis followed by MS3 analysis. For MS2 spectra, ions were isolated using a
997 0.5 m/z window using the mass filter. The MS2 scan was performed in the quadrupole ion trap
998 (CID, AGC 1 x 10^4, normalized collision energy 30%, max injection time 35 ms) and the MS3
999 scan was analyzed in the Orbitrap (HCD, 60k resolution, max AGC 5x10^4, max injection time
1000 250 ms, normalized collision energy 50). For TMT reporter ion quantification, up to six fragment
1001 ions from each MS2 spectrum were selected for MS3 analysis using synchronous precursor
1002 selection (SPS).
1003
1004 Mass spectrometry data were processed using an in-house software pipeline [71]. Raw files were
1005 converted to mzXML files and searched against a composite human uniprot database (downloaded
1006 on 29th March 2017) containing sequences in forward and reverse orientations using the Sequest
1007 algorithm. Database searching matched MS/MS spectra with fully tryptic peptides from this
1008 composite dataset with a precursor ion tolerance of 20 ppm and a product ion tolerance of 0.6 Da.
1009 Carbamidomethylation of cysteine residues (+57.02146 Da) and TMT tags of peptide N-termini
1010 (+229.162932 Da) were set as static modifications. Oxidation of methionines (+15.99492 Da) was
1011 set as a variable modification. Linear discriminant analysis was used to filter peptide spectral
1012 matches to a 1 % FDR (false discovery rate) as described previously [71]. Non-unique peptides that
1013 matched to multiple proteins were assigned to proteins that contained the largest number of
1014 matched redundant peptides sequences using the principle of Occam's razor [71].
1015
1016 Quantification of TMT reporter ion intensities was performed by extracting the most intense ion
1017 within a 0.003 m/z window at the predicted m/z value for each reporter ion. TMT spectra were
1018 used for quantification when the sum of the signal-to-noise for all the reporter ions was greater
1019 than 200 and the isolation specificity was greater than 0.75 [72].
1020
1021 Base 2 logarithm of protein fold-changes were estimated by fitting a previously described Bayesian
1022 model [73] to the peptide level intensities. Protein estimates are reported as the mean of the posterior
1023 distribution for each parameter. Similarly, coefficients of variation are calculated by taking the

posterior variance divided by the posterior mean. The probability of a small change ("P_null") was estimated as the frequency of posterior samples that fall within the interval (-1,1) on the log2 scale.

Acknowledgements

We thank Jonathan Paw for flow cytometry and cell sorting; Margaret Roy, Andrea Ireland, Twaritha Vijay, Nicole Fong for next-generation sequencing; Adam Baker and Matt Sooknah for RNA-seq data visualization; Hugo Hilton, David Stokoe, and Robert Cohen for critical reading of the manuscript; and members of the Calico Oncology group for helpful discussion.

Competing Interests

All authors are employees of Calico Life Sciences, LLC.

References

1 Snyder, A. *et al.* Genetic basis for clinical response to CTLA-4 blockade in melanoma. *N Engl J Med* **371**, 2189-2199, doi:10.1056/NEJMoa1406498 (2014).

2 Tumeh, P. C. *et al.* PD-1 blockade induces responses by inhibiting adaptive immune resistance. *Nature* **515**, 568-571, doi:10.1038/nature13954 (2014).

3 Mariathasan, S. *et al.* TGFbeta attenuates tumour response to PD-L1 blockade by contributing to exclusion of T cells. *Nature* **554**, 544-548, doi:10.1038/nature25501 (2018).

4 Galon, J. & Bruni, D. Approaches to treat immune hot, altered and cold tumours with combination immunotherapies. *Nat Rev Drug Discov*, doi:10.1038/s41573-018-0007-y (2019).

5 Easwaran, H., Tsai, H. C. & Baylin, S. B. Cancer epigenetics: tumor heterogeneity, plasticity of stem-like states, and drug resistance. *Mol Cell* **54**, 716-727, doi:10.1016/j.molcel.2014.05.015 (2014).

6 Zaretsky, J. M. *et al.* Mutations Associated with Acquired Resistance to PD-1 Blockade in Melanoma. *N Engl J Med* **375**, 819-829, doi:10.1056/NEJMoa1604958 (2016).

7 Sade-Feldman, M. *et al.* Resistance to checkpoint blockade therapy through inactivation of antigen presentation. *Nat Commun* **8**, 1136, doi:10.1038/s41467-017-01062-w (2017).

8 Kearney, C. J. *et al.* Tumor immune evasion arises through loss of TNF sensitivity. *Sci Immunol* **3**, doi:10.1126/sciimmunol.aar3451 (2018).

9 Pan, D. *et al.* A major chromatin regulator determines resistance of tumor cells to T cell-mediated killing. *Science* **359**, 770-775, doi:10.1126/science.aao1710 (2018).

10 Manguso, R. T. *et al.* In vivo CRISPR screening identifies Ptpn2 as a cancer immunotherapy target. *Nature* **547**, 413-418, doi:10.1038/nature23270 (2017).

1062 11 Patel, S. J. *et al.* Identification of essential genes for cancer immunotherapy. *Nature* **548**,
1063 537-542, doi:10.1038/nature23477 (2017).
1064 12 Dunn, G. P., Old, L. J. & Schreiber, R. D. The immunobiology of cancer
1065 immunosurveillance and immunoediting. *Immunity* **21**, 137-148,
1066 doi:10.1016/j.immuni.2004.07.017 (2004).
1067 13 Rodig, S. J. *et al.* MHC proteins confer differential sensitivity to CTLA-4 and PD-1
1068 blockade in untreated metastatic melanoma. *Sci Transl Med* **10**,
1069 doi:10.1126/scitranslmed.aar3342 (2018).
1070 14 Gao, J. *et al.* Loss of IFN-gamma Pathway Genes in Tumor Cells as a Mechanism of
1071 Resistance to Anti-CTLA-4 Therapy. *Cell* **167**, 397-404 e399,
1072 doi:10.1016/j.cell.2016.08.069 (2016).
1073 15 McGranahan, N. *et al.* Allele-Specific HLA Loss and Immune Escape in Lung Cancer
1074 Evolution. *Cell* **171**, 1259-1271 e1211, doi:10.1016/j.cell.2017.10.001 (2017).
1075 16 Marcus, A. *et al.* Recognition of tumors by the innate immune system and natural killer
1076 cells. *Adv Immunol* **122**, 91-128, doi:10.1016/B978-0-12-800267-4.00003-1 (2014).
1077 17 Moynihan, K. D. *et al.* Eradication of large established tumors in mice by combination
1078 immunotherapy that engages innate and adaptive immune responses. *Nat Med* **22**,
1079 1402-1410, doi:10.1038/nm.4200 (2016).
1080 18 Lopez-Soto, A., Gonzalez, S., Smyth, M. J. & Galluzzi, L. Control of Metastasis by NK Cells.
1081 *Cancer Cell* **32**, 135-154, doi:10.1016/j.ccell.2017.06.009 (2017).
1082 19 Chiossone, L., Dumas, P. Y., Vienne, M. & Vivier, E. Natural killer cells and other innate
1083 lymphoid cells in cancer. *Nat Rev Immunol* **18**, 671-688, doi:10.1038/s41577-018-0061-z
1084 (2018).
1085 20 Ljunggren, H. G. & Malmberg, K. J. Prospects for the use of NK cells in immunotherapy of
1086 human cancer. *Nat Rev Immunol* **7**, 329-339, doi:10.1038/nri2073 (2007).
1087 21 Klingemann, H. G. *et al.* Establishment and characterization of a human leukemic cell
1088 line (SR-91) with features suggestive of early hematopoietic progenitor cell origin. *Leuk*
1089 *Lymphoma* **12**, 463-470, doi:10.3109/10428199409073789 (1994).
1090 22 Maki, G., Klingemann, H. G., Martinson, J. A. & Tam, Y. K. Factors regulating the
1091 cytotoxic activity of the human natural killer cell line, NK-92. *J Hematother Stem Cell Res*
1092 **10**, 369-383, doi:10.1089/152581601750288975 (2001).
1093 23 Li, W. *et al.* MAGeCK enables robust identification of essential genes from genome-scale
1094 CRISPR/Cas9 knockout screens. *Genome Biol* **15**, 554, doi:10.1186/s13059-014-0554-4
1095 (2014).
1096 24 Brandt, C. S. *et al.* The B7 family member B7-H6 is a tumor cell ligand for the activating
1097 natural killer cell receptor NKp30 in humans. *J Exp Med* **206**, 1495-1503,
1098 doi:10.1084/jem.20090681 (2009).
1099 25 Selvaraj, P. *et al.* The T lymphocyte glycoprotein CD2 binds the cell surface ligand LFA-3.
1100 *Nature* **326**, 400-403, doi:10.1038/326400a0 (1987).
1101 26 Rolle, A. *et al.* CD2-CD58 interactions are pivotal for the activation and function of
1102 adaptive natural killer cells in human cytomegalovirus infection. *Eur J Immunol* **46**, 2420-
1103 2425, doi:10.1002/eji.201646492 (2016).

1104 27 Martin, M. *et al.* CD84 functions as a homophilic adhesion molecule and enhances IFN-
1105 gamma secretion: adhesion is mediated by Ig-like domain 1. *J Immunol* **167**, 3668-3676
1106 (2001).
1107 28 Veillette, A. Immune regulation by SLAM family receptors and SAP-related adaptors. *Nat*
1108 *Rev Immunol* **6**, 56-66, doi:10.1038/nri1761 (2006).
1109 29 Stanietsky, N. *et al.* The interaction of TIGIT with PVR and PVRL2 inhibits human NK cell
1110 cytotoxicity. *Proc Natl Acad Sci U S A* **106**, 17858-17863, doi:10.1073/pnas.0903474106
1111 (2009).
1112 30 Bottino, C. *et al.* Identification of PVR (CD155) and Nectin-2 (CD112) as cell surface
1113 ligands for the human DNAM-1 (CD226) activating molecule. *J Exp Med* **198**, 557-567,
1114 doi:10.1084/jem.20030788 (2003).
1115 31 Chen, E., Karr, R. W., Frost, J. P., Gonwa, T. A. & Ginder, G. D. Gamma interferon and 5-
1116 azacytidine cause transcriptional elevation of class I major histocompatibility complex
1117 gene expression in K562 leukemia cells in the absence of differentiation. *Mol Cell Biol* **6**,
1118 1698-1705 (1986).
1119 32 Jin, J., Arias, E. E., Chen, J., Harper, J. W. & Walter, J. C. A family of diverse Cul4-Ddb1-
1120 interacting proteins includes Cdt2, which is required for S phase destruction of the
1121 replication factor Cdt1. *Mol Cell* **23**, 709-721, doi:10.1016/j.molcel.2006.08.010 (2006).
1122 33 Jackson, S. & Xiong, Y. CRL4s: the CUL4-RING E3 ubiquitin ligases. *Trends Biochem Sci* **34**,
1123 562-570, doi:10.1016/j.tibs.2009.07.002 (2009).
1124 34 Uhlmann, F. SMC complexes: from DNA to chromosomes. *Nat Rev Mol Cell Biol* **17**, 399-
1125 412, doi:10.1038/nrm.2016.30 (2016).
1126 35 Mazumdar, C. & Majeti, R. The role of mutations in the cohesin complex in acute
1127 myeloid leukemia. *Int J Hematol* **105**, 31-36, doi:10.1007/s12185-016-2119-7 (2017).
1128 36 Chen, L. & Flies, D. B. Molecular mechanisms of T cell co-stimulation and co-inhibition.
1129 *Nat Rev Immunol* **13**, 227-242, doi:10.1038/nri3405 (2013).
1130 37 Acuto, O. & Michel, F. CD28-mediated co-stimulation: a quantitative support for TCR
1131 signalling. *Nat Rev Immunol* **3**, 939-951, doi:10.1038/nri1248 (2003).
1132 38 Wilson, J. L. *et al.* NK cell triggering by the human costimulatory molecules CD80 and
1133 CD86. *J Immunol* **163**, 4207-4212 (1999).
1134 39 Galea-Lauri, J. *et al.* Expression of a variant of CD28 on a subpopulation of human NK
1135 cells: implications for B7-mediated stimulation of NK cells. *J Immunol* **163**, 62-70 (1999).
1136 40 Chambers, B. J., Salcedo, M. & Ljunggren, H. G. Triggering of natural killer cells by the
1137 costimulatory molecule CD80 (B7-1). *Immunity* **5**, 311-317 (1996).
1138 41 Azuma, M., Cayabyab, M., Buck, D., Phillips, J. H. & Lanier, L. L. Involvement of CD28 in
1139 MHC-unrestricted cytotoxicity mediated by a human natural killer leukemia cell line. *J*
1140 *Immunol* **149**, 1115-1123 (1992).
1141 42 Martin-Fontecha, A., Assarsson, E., Carbone, E., Karre, K. & Ljunggren, H. G. Triggering of
1142 murine NK cells by CD40 and CD86 (B7-2). *J Immunol* **162**, 5910-5916 (1999).
1143 43 Lindner, I. *et al.* Induced dendritic cell differentiation of chronic myeloid leukemia blasts
1144 is associated with down-regulation of BCR-ABL. *J Immunol* **171**, 1780-1791 (2003).
1145 44 Townsend, S. E. & Allison, J. P. Tumor rejection after direct costimulation of CD8+ T cells
1146 by B7-transfected melanoma cells. *Science* **259**, 368-370 (1993).

1147 45 Chen, L. *et al.* Costimulation of antitumor immunity by the B7 counterreceptor for the T
1148 lymphocyte molecules CD28 and CTLA-4. *Cell* **71**, 1093-1102 (1992).
1149 46 Peach, R. J. *et al.* Both extracellular immunoglobin-like domains of CD80 contain
1150 residues critical for binding T cell surface receptors CTLA-4 and CD28. *J Biol Chem* **270**,
1151 21181-21187 (1995).
1152 47 Assi, R. *et al.* Final results of a phase 2, open-label study of indisulam, idarubicin, and
1153 cytarabine in patients with relapsed or refractory acute myeloid leukemia and high-risk
1154 myelodysplastic syndrome. *Cancer* **124**, 2758-2765, doi:10.1002/cncr.31398 (2018).
1155 48 Han, T. *et al.* Anticancer sulfonamides target splicing by inducing RBM39 degradation via
1156 recruitment to DCAF15. *Science* **356**, doi:10.1126/science.aal3755 (2017).
1157 49 Uehara, T. *et al.* Selective degradation of splicing factor CAPERalpha by anticancer
1158 sulfonamides. *Nat Chem Biol* **13**, 675-680, doi:10.1038/nchembio.2363 (2017).
1159 50 Ito, T. *et al.* Identification of a primary target of thalidomide teratogenicity. *Science* **327**,
1160 1345-1350, doi:10.1126/science.1177319 (2010).
1161 51 Fischer, E. S. *et al.* Structure of the DDB1-CRBN E3 ubiquitin ligase in complex with
1162 thalidomide. *Nature* **512**, 49-53, doi:10.1038/nature13527 (2014).
1163 52 Kronke, J. *et al.* Lenalidomide causes selective degradation of IKZF1 and IKZF3 in
1164 multiple myeloma cells. *Science* **343**, 301-305, doi:10.1126/science.1244851 (2014).
1165 53 Bolouri, H. *et al.* The molecular landscape of pediatric acute myeloid leukemia reveals
1166 recurrent structural alterations and age-specific mutational interactions. *Nat Med* **24**,
1167 103-112, doi:10.1038/nm.4439 (2018).
1168 54 Cancer Genome Atlas Research, N. *et al.* Genomic and epigenomic landscapes of adult
1169 de novo acute myeloid leukemia. *N Engl J Med* **368**, 2059-2074,
1170 doi:10.1056/NEJMoa1301689 (2013).
1171 55 Roux, K. J., Kim, D. I., Raida, M. & Burke, B. A promiscuous biotin ligase fusion protein
1172 identifies proximal and interacting proteins in mammalian cells. *J Cell Biol* **196**, 801-810,
1173 doi:10.1083/jcb.201112098 (2012).
1174 56 Luo, N. *et al.* Melanoma response to anti-PD-L1 immunotherapy requires JAK1 signaling,
1175 but not JAK2. *Oncoimmunology* **7**, e1438106, doi:10.1080/2162402X.2018.1438106
1176 (2018).
1177 57 O'Connell, B. C. & Harper, J. W. Ubiquitin proteasome system (UPS): what can chromatin
1178 do for you? *Curr Opin Cell Biol* **19**, 206-214, doi:10.1016/j.ceb.2007.02.014 (2007).
1179 58 Litwin, I., Pilarczyk, E. & Wysocki, R. The Emerging Role of Cohesin in the DNA Damage
1180 Response. *Genes (Basel)* **9**, doi:10.3390/genes9120581 (2018).
1181 59 Chandrashekar, D. S. *et al.* UALCAN: A Portal for Facilitating Tumor Subgroup Gene
1182 Expression and Survival Analyses. *Neoplasia* **19**, 649-658, doi:10.1016/j.neo.2017.05.002
1183 (2017).
1184 60 Doench, J. G. *et al.* Optimized sgRNA design to maximize activity and minimize off-target
1185 effects of CRISPR-Cas9. *Nat Biotechnol* **34**, 184-191, doi:10.1038/nbt.3437 (2016).
1186 61 Sanjana, N. E., Shalem, O. & Zhang, F. Improved vectors and genome-wide libraries for
1187 CRISPR screening. *Nat Methods* **11**, 783-784, doi:10.1038/nmeth.3047 (2014).
1188 62 Grigaite, R., Maneliene, Z. & Janulaitis, A. AarI, a restriction endonuclease from
1189 Arthrobacter aurescens SS2-322, which recognizes the novel non-palindromic sequence
1190 5'-CACCTGC(N)4/8-3'. *Nucleic Acids Res* **30**, e123 (2002).

1191 63 Chen, B. *et al.* Dynamic imaging of genomic loci in living human cells by an optimized
1192 CRISPR/Cas system. *Cell* **155**, 1479-1491, doi:10.1016/j.cell.2013.12.001 (2013).
1193 64 van Overbeek, M. *et al.* DNA Repair Profiling Reveals Nonrandom Outcomes at Cas9-
1194 Mediated Breaks. *Mol Cell* **63**, 633-646, doi:10.1016/j.molcel.2016.06.037 (2016).
1195 65 Stamper, C. C. *et al.* Crystal structure of the B7-1/CTLA-4 complex that inhibits human
1196 immune responses. *Nature* **410**, 608-611, doi:10.1038/35069118 (2001).
1197 66 Patro, R., Duggal, G., Love, M. I., Irizarry, R. A. & Kingsford, C. Salmon provides fast and
1198 bias-aware quantification of transcript expression. *Nat Methods* **14**, 417-419,
1199 doi:10.1038/nmeth.4197 (2017).
1200 67 Pimentel, H., Bray, N. L., Puente, S., Melsted, P. & Pachter, L. Differential analysis of
1201 RNA-seq incorporating quantification uncertainty. *Nat Methods* **14**, 687-690,
1202 doi:10.1038/nmeth.4324 (2017).
1203 68 Barretina, J. *et al.* The Cancer Cell Line Encyclopedia enables predictive modelling of
1204 anticancer drug sensitivity. *Nature* **483**, 603-607, doi:10.1038/nature11003 (2012).
1205 69 Rappsilber, J., Mann, M. & Ishihama, Y. Protocol for micro-purification, enrichment, pre-
1206 fractionation and storage of peptides for proteomics using StageTips. *Nat Protoc* **2**,
1207 1896-1906, doi:10.1038/nprot.2007.261 (2007).
1208 70 Edwards, A. & Haas, W. Multiplexed Quantitative Proteomics for High-Throughput
1209 Comprehensive Proteome Comparisons of Human Cell Lines. *Methods Mol Biol* **1394**, 1-
1210 13, doi:10.1007/978-1-4939-3341-9_1 (2016).
1211 71 Huttlin, E. L. *et al.* A tissue-specific atlas of mouse protein phosphorylation and
1212 expression. *Cell* **143**, 1174-1189, doi:10.1016/j.cell.2010.12.001 (2010).
1213 72 Ting, L., Rad, R., Gygi, S. P. & Haas, W. MS3 eliminates ratio distortion in isobaric
1214 multiplexed quantitative proteomics. *Nat Methods* **8**, 937-940, doi:10.1038/nmeth.1714
1215 (2011).
1216 73 O'Brien, J. J. *et al.* Compositional Proteomics: Effects of Spatial Constraints on Protein
1217 Quantification Utilizing Isobaric Tags. *J Proteome Res* **17**, 590-599,
1218 doi:10.1021/acs.jproteome.7b00699 (2018).
1219

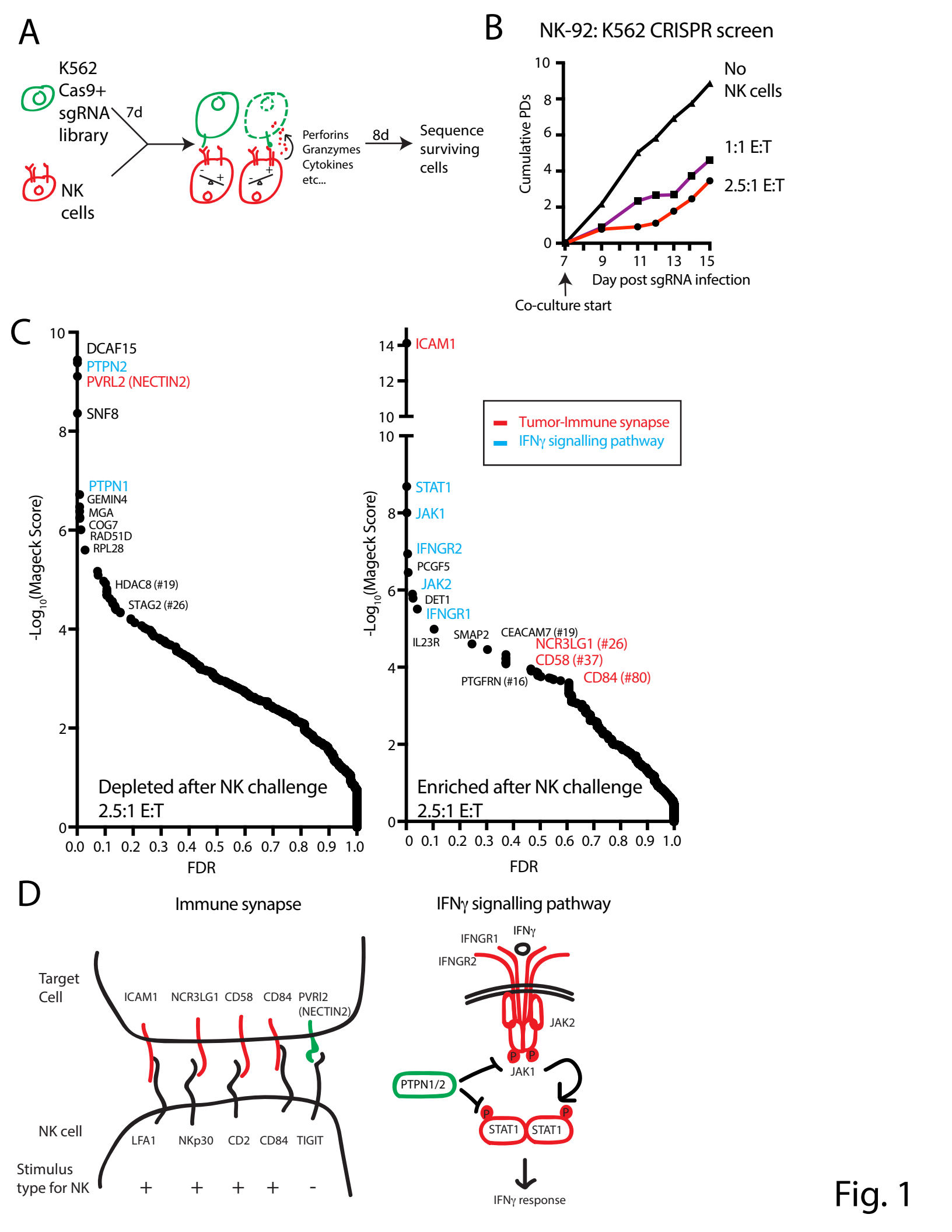
A
K562
Cas9+
sgRNA
library
NK
cells
7d
Perforins
Granzymes
Cytokines
etc...
8d
Sequence
surviving
cells
B
NK-92: K562 CRISPR screen
Cumulative PDs
No
NK cells
1:1 E:T
2.5:1 E:T
Day post sgRNA infection
Co-culture start
C
DCAF15
PTPN2
PVRL2 (NECTIN2)
SNF8
PTPN1
GEMIN4
MGA
COG7
RAD51D
RPL28
HDAC8 (#19)
STAG2 (#26)
-Log10(Mageck Score)
Depleted after NK challenge
2.5:1 E:T
FDR
ICAM1
Tumor-Immune synapse
IFNγ signalling pathway
STAT1
JAK1
IFNGR2
PCGF5
JAK2
DET1
IFNGR1
IL23R
SMAP2
CEACAM7 (#19)
NCR3LG1 (#26)
CD58 (#37)
CD84 (#80)
PTGFRN (#16)
Enriched after NK challenge
2.5:1 E:T
D
Immune synapse
Target
Cell
ICAM1
NCR3LG1
CD58
CD84
PVRl2
(NECTIN2)
NK cell
LFA1
NKp30
CD2
CD84
TIGIT
Stimulus
type for NK
+
+
+
+
-
IFNγ signalling pathway
IFNγ
IFNGR1
IFNGR2
JAK2
JAK1
PTPN1/2
P
STAT1
STAT1
IFNγ response

Fig. 1

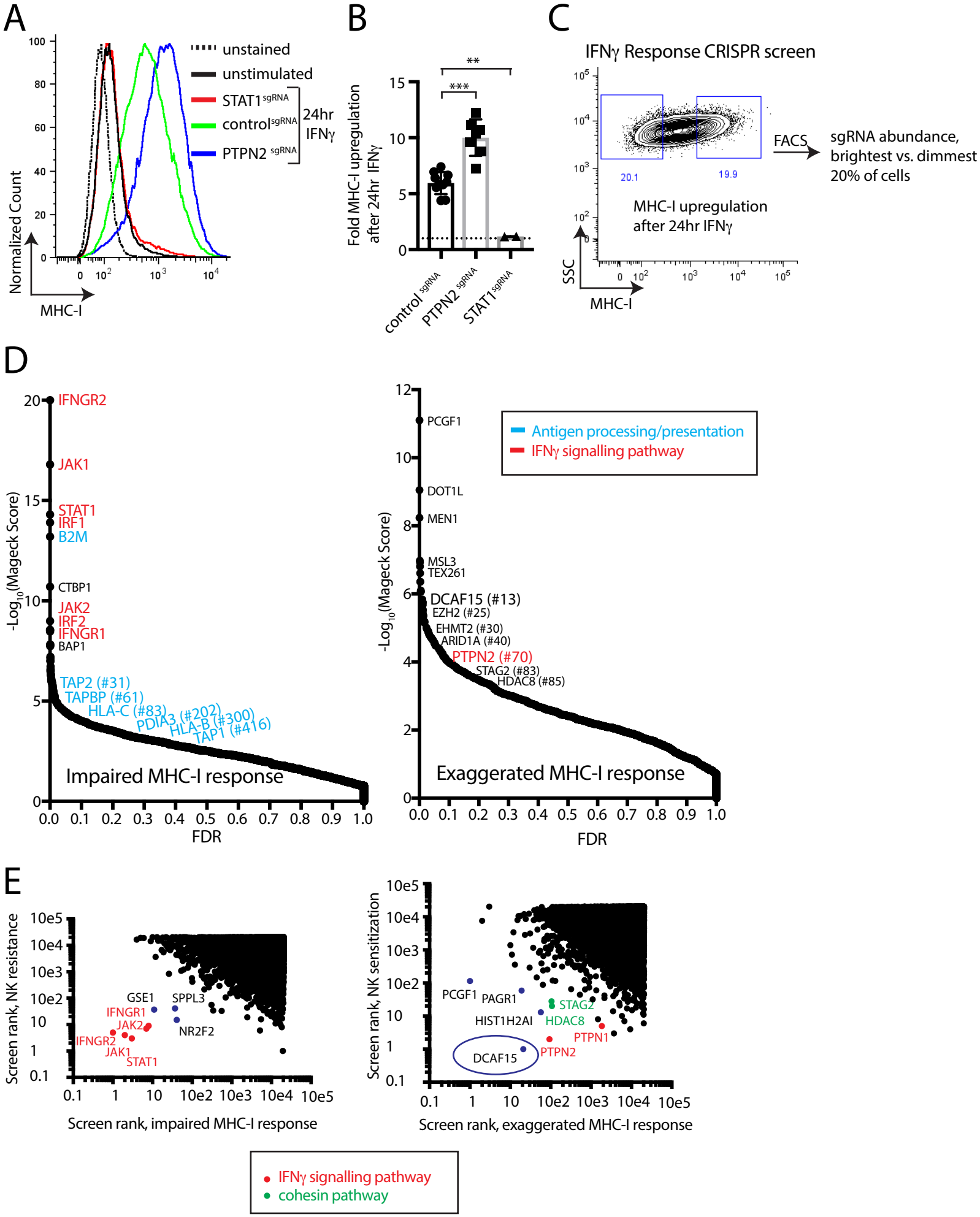
A
unstained
unstimulated
STAT1 sgRNA
control sgRNA
PTPN2 sgRNA
24hr IFNγ
Normalized Count
MHC-I
B
Fold MHC-I upregulation after 24hr IFNγ
control sgRNA
PTPN2 sgRNA
STAT1 sgRNA
C
IFNγ Response CRISPR screen
20.1
19.9
MHC-I upregulation after 24hr IFNγ
FACS
sgRNA abundance, brightest vs. dimmest 20% of cells
SSC
MHC-I
D
IFNGR2
JAK1
STAT1
IRF1
B2M
CTBP1
JAK2
IRF2
IFNGR1
BAP1
TAP2 (#31)
TAPBP (#61)
HLA-C (#83)
PDIA3 (#202)
HLA-B (#300)
TAP1 (#416)
Impaired MHC-I response
-Log10(Mageck Score)
FDR
Antigen processing/presentation
IFNγ signalling pathway
PCGF1
DOT1L
MEN1
MSL3
TEX261
DCAF15 (#13)
EZH2 (#25)
EHMT2 (#30)
ARID1A (#40)
PTPN2 (#70)
STAG2 (#83)
HDAC8 (#85)
Exaggerated MHC-I response
E
Screen rank, NK resistance
GSE1
SPPL3
IFNGR1
JAK2
NR2F2
IFNGR2
JAK1
STAT1
Screen rank, impaired MHC-I response
Screen rank, NK sensitization
PCGF1
PAGR1
STAG2
HIST1H2AI
HDAC8
PTPN1
DCAF15
PTPN2
Screen rank, exaggerated MHC-I response
IFNγ signalling pathway
cohesin pathway

Fig. 2

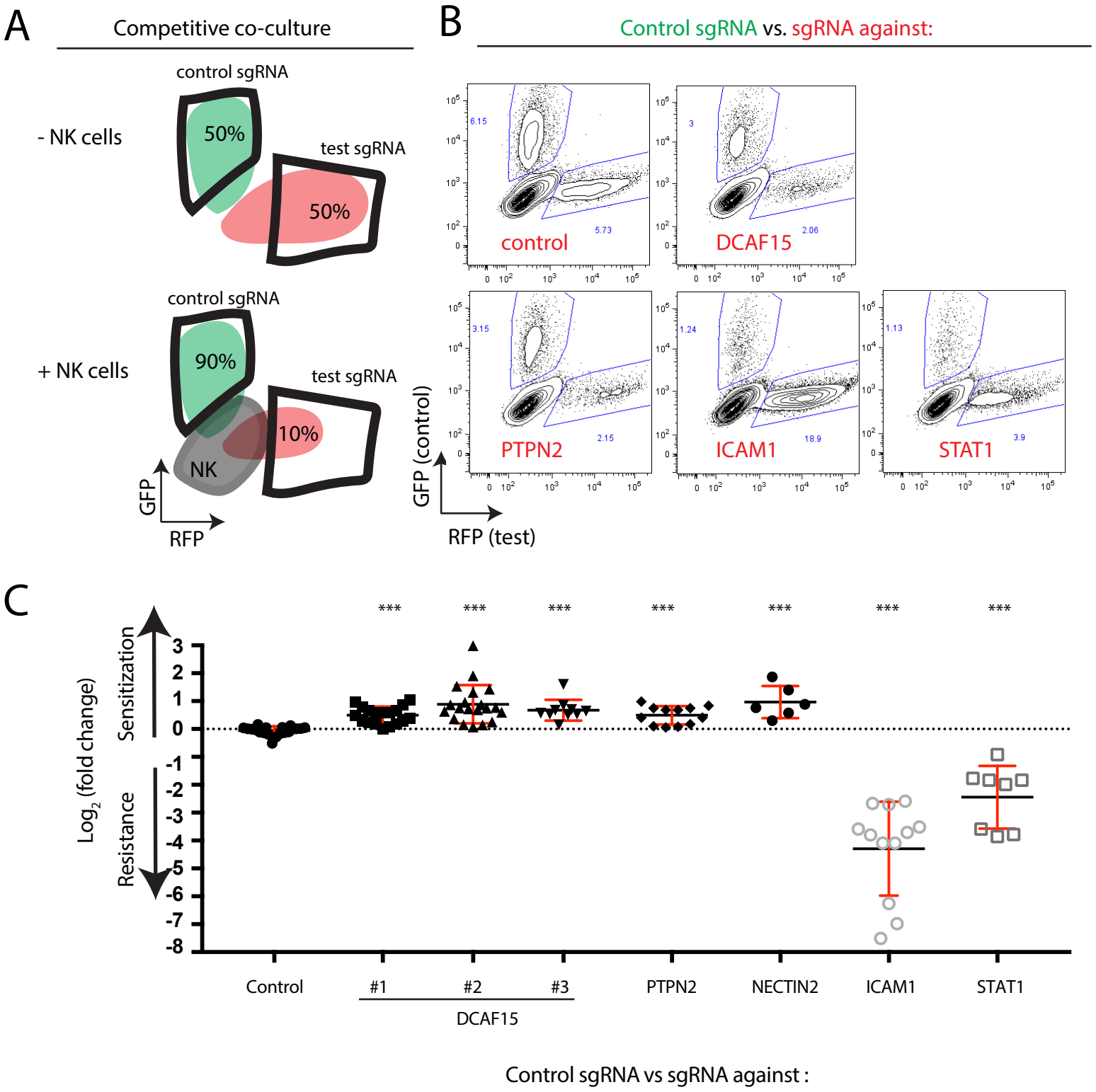
A
Competitive co-culture
control sgRNA
- NK cells
50%
test sgRNA
50%
control sgRNA
+ NK cells
90%
test sgRNA
10%
NK
GFP
RFP
B
Control sgRNA vs. sgRNA against:
control
DCAF15
PTPN2
ICAM1
STAT1
GFP (control)
RFP (test)
C
Sensitization
Resistance
Log2 (fold change)
Control
#1
#2
#3
DCAF15
PTPN2
NECTIN2
ICAM1
STAT1
Control sgRNA vs sgRNA against :

Fig. 3

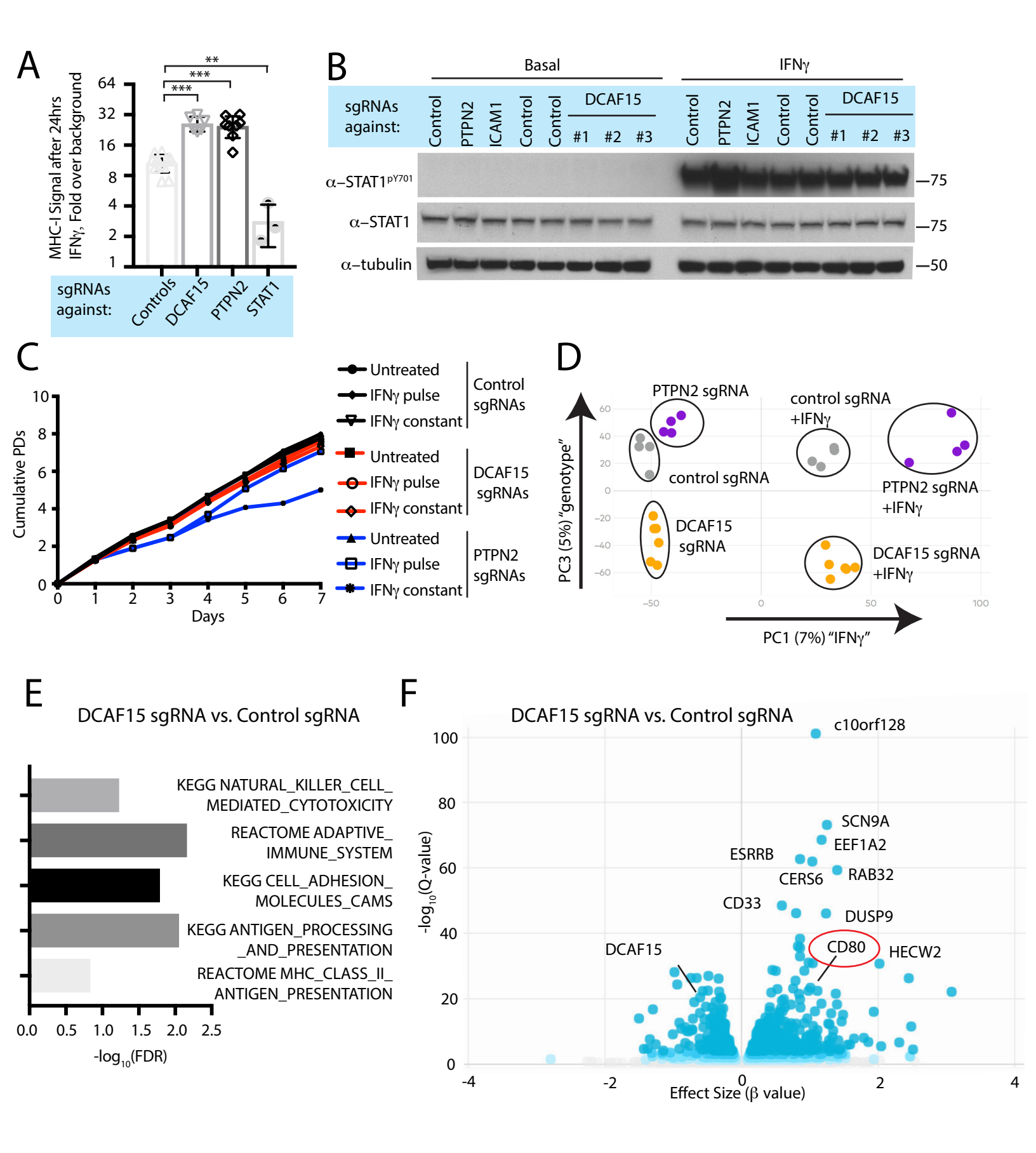
A
MHC-I Signal after 24hrs IFNγ, Fold over background
64
32
16
8
4
2
1
**
***
***
sgRNAs against:
Controls
DCAF15
PTPN2
STAT1
B
Basal
IFNγ
sgRNAs against:
Control
PTPN2
ICAM1
Control
Control
DCAF15
#1
#2
#3
α–STAT1pY701
α–STAT1
α–tubulin
—75
—75
—50
C
Cumulative PDs
Days
Untreated
IFNγ pulse
IFNγ constant
Control sgRNAs
DCAF15 sgRNAs
PTPN2 sgRNAs
D
PTPN2 sgRNA
control sgRNA
control sgRNA +IFNγ
PTPN2 sgRNA +IFNγ
DCAF15 sgRNA
DCAF15 sgRNA +IFNγ
PC3 (5%) "genotype"
PC1 (7%) "IFNγ"
E
DCAF15 sgRNA vs. Control sgRNA
KEGG NATURAL_KILLER_CELL_MEDIATED_CYTOTOXICITY
REACTOME ADAPTIVE_IMMUNE_SYSTEM
KEGG CELL_ADHESION_MOLECULES_CAMS
KEGG ANTIGEN_PROCESSING_AND_PRESENTATION
REACTOME MHC_CLASS_II_ANTIGEN_PRESENTATION
-log10(FDR)
F
DCAF15 sgRNA vs. Control sgRNA
c10orf128
SCN9A
EEF1A2
ESRRB
CERS6
RAB32
CD33
DUSP9
CD80
HECW2
DCAF15
-log10(Q-value)
Effect Size (β value)

Fig. 4

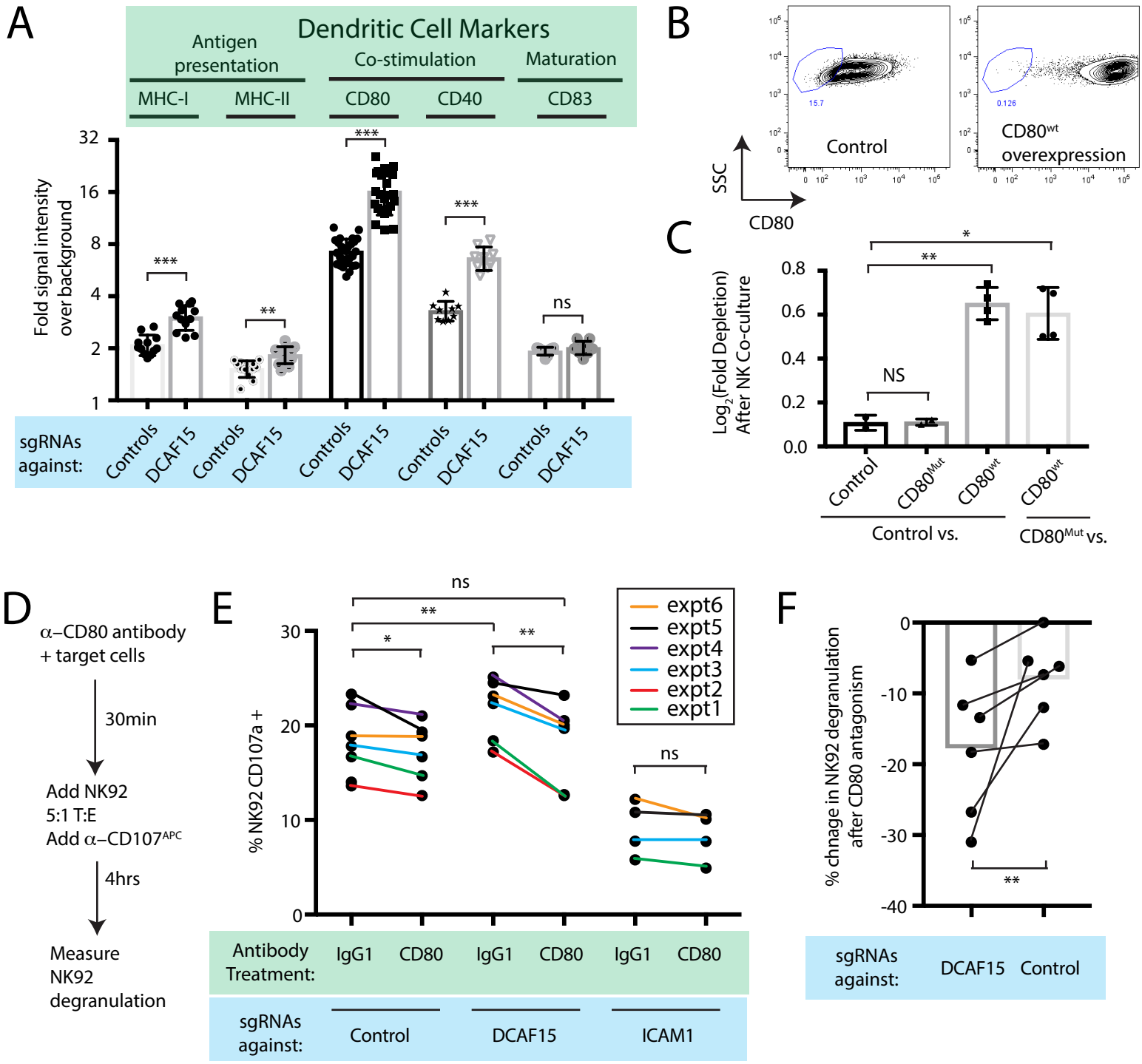
A
Dendritic Cell Markers
Antigen presentation
Co-stimulation
Maturation
MHC-I
MHC-II
CD80
CD40
CD83
Fold signal intensity over background
32
16
8
4
2
1
***
**
***
***
ns
sgRNAs against:
Controls
DCAF15
B
SSC
CD80
Control
CD80wt overexpression
C
Log2(Fold Depletion) After NK Co-culture
0.8
0.6
0.4
0.2
0.0
*
**
NS
Control
CD80Mut
CD80wt
Control vs.
CD80Mut vs.
D
α–CD80 antibody + target cells
30min
Add NK92 5:1 T:E
Add α–CD107APC
4hrs
Measure NK92 degranulation
E
% NK92 CD107a +
30
20
10
0
ns
**
*
expt6
expt5
expt4
expt3
expt2
expt1
Antibody Treatment:
IgG1
CD80
sgRNAs against:
Control
DCAF15
ICAM1
F
% chnage in NK92 degranulation after CD80 antagonism
0
-10
-20
-30
-40
sgRNAs against:
DCAF15
Control

Fig. 5

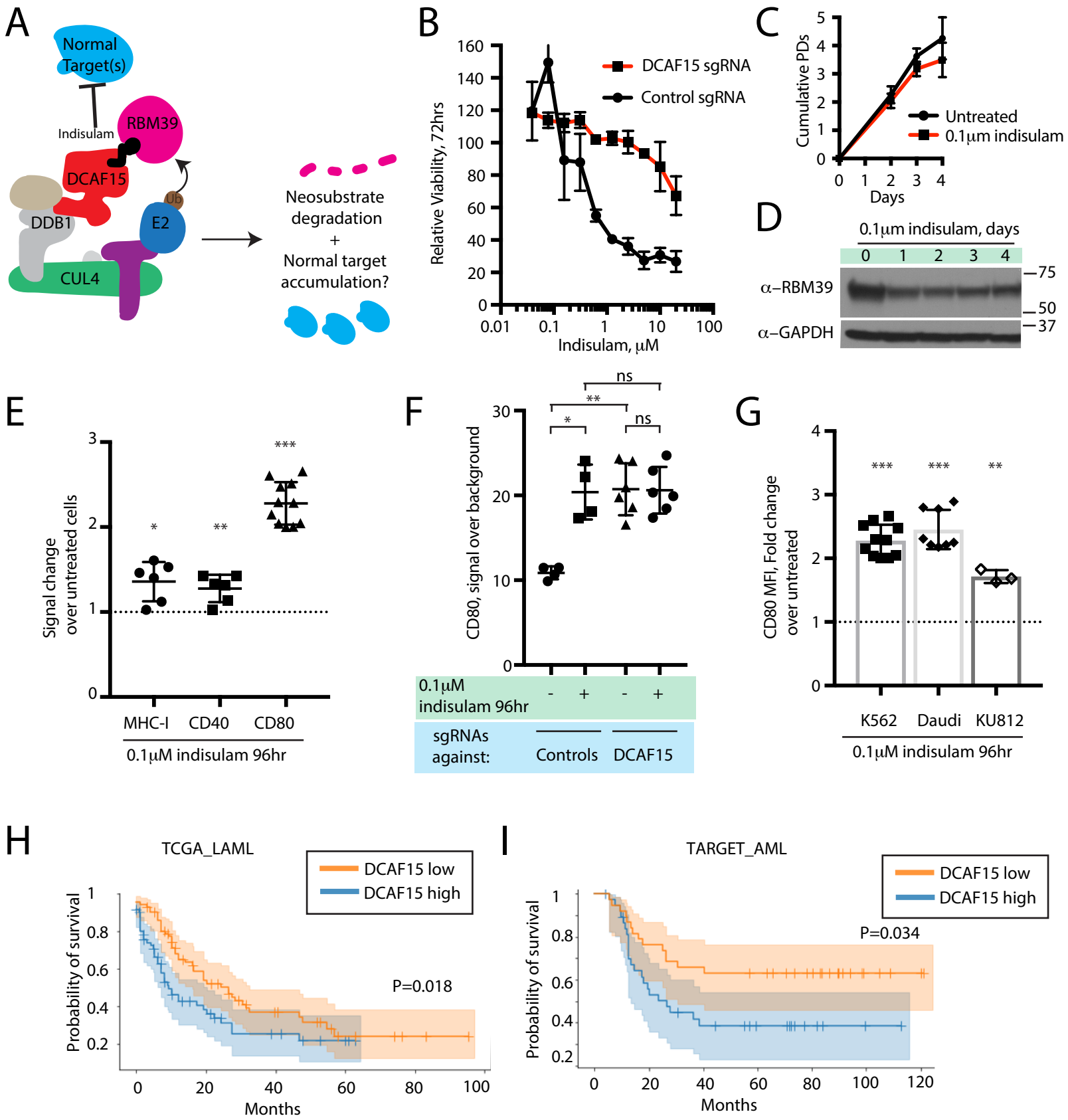
A
Normal Target(s)
Indisulam
RBM39
DCAF15
DDB1
E2
Ub
CUL4
Neosubstrate degradation + Normal target accumulation?
B
DCAF15 sgRNA
Control sgRNA
Relative Viability, 72hrs
Indisulam, μM
C
Cumulative PDs
Untreated
0.1μm indisulam
Days
D
0.1μm indisulam, days
0 1 2 3 4
α–RBM39
α–GAPDH
75
50
37
E
Signal change over untreated cells
MHC-I
CD40
CD80
0.1μM indisulam 96hr
F
CD80, signal over background
ns
**
*
ns
0.1μM indisulam 96hr
sgRNAs against:
Controls
DCAF15
G
CD80 MFI, Fold change over untreated
K562
Daudi
KU812
0.1μM indisulam 96hr
H
TCGA_LAML
DCAF15 low
DCAF15 high
Probability of survival
P=0.018
Months
I
TARGET_AML
DCAF15 low
DCAF15 high
Probability of survival
P=0.034
Months

Fig. 6

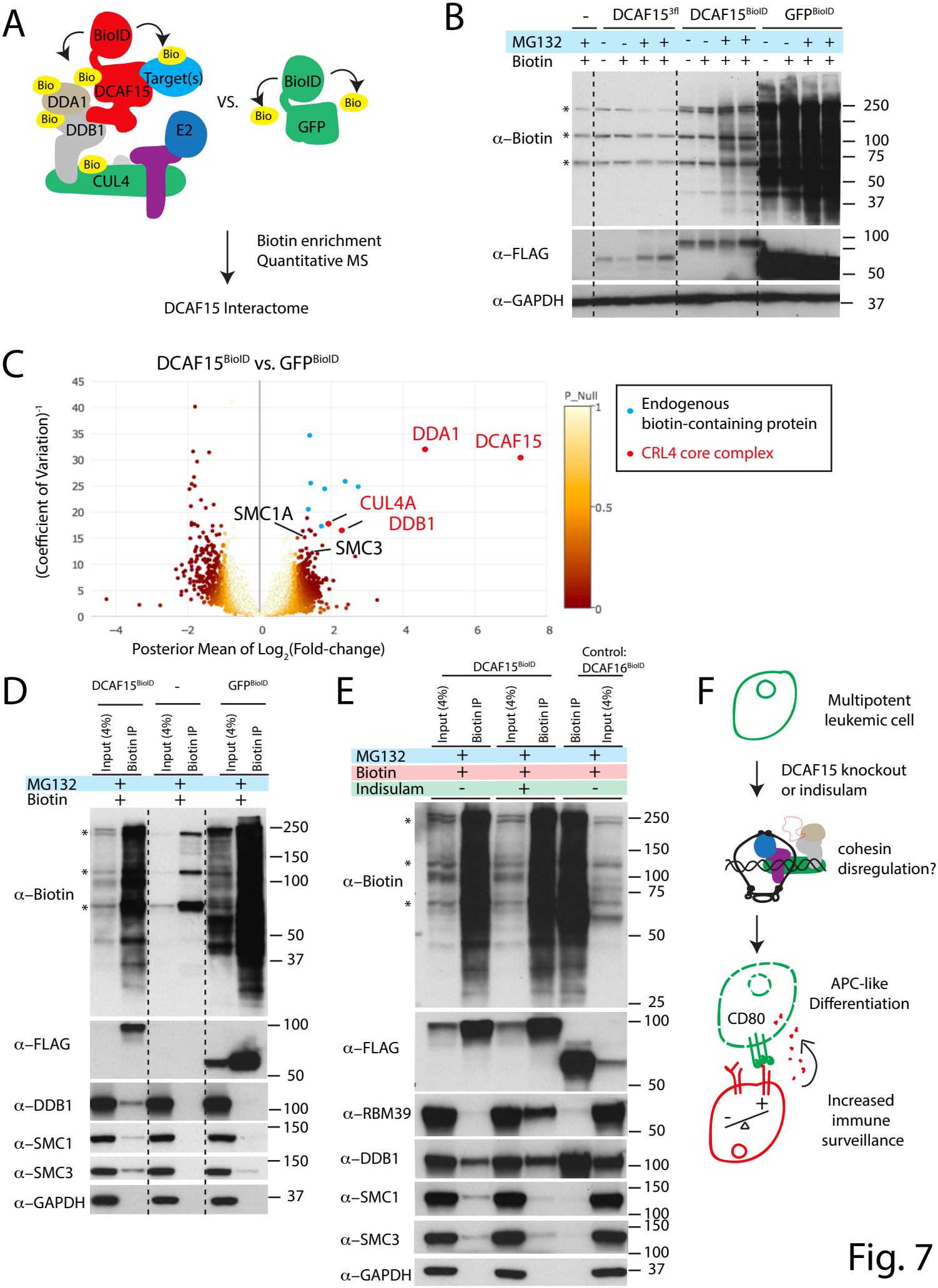
A
BioID
Bio
Target(s)
DCAF15
DDA1
DDB1
E2
CUL4
VS.
GFP
Biotin enrichment
Quantitative MS
DCAF15 Interactome
B
DCAF15^3fl
DCAF15^BioID
GFP^BioID
MG132
Biotin
α–Biotin
α–FLAG
α–GAPDH
250
100
75
50
37
C
DCAF15^BioID vs. GFP^BioID
(Coefficient of Variation)^-1
Posterior Mean of Log2(Fold-change)
P_Null
DDA1
DCAF15
CUL4A
DDB1
SMC1A
SMC3
Endogenous biotin-containing protein
CRL4 core complex
D
DCAF15^BioID
GFP^BioID
Input (4%)
Biotin IP
α–Biotin
α–FLAG
α–DDB1
α–SMC1
α–SMC3
α–GAPDH
E
DCAF15^BioID
Control: DCAF16^BioID
MG132
Biotin
Indisulam
α–Biotin
α–FLAG
α–RBM39
α–DDB1
α–SMC1
α–SMC3
α–GAPDH
F
Multipotent leukemic cell
DCAF15 knockout or indisulam
cohesin disregulation?
APC-like Differentiation
CD80
Increased immune surveillance

Fig. 7

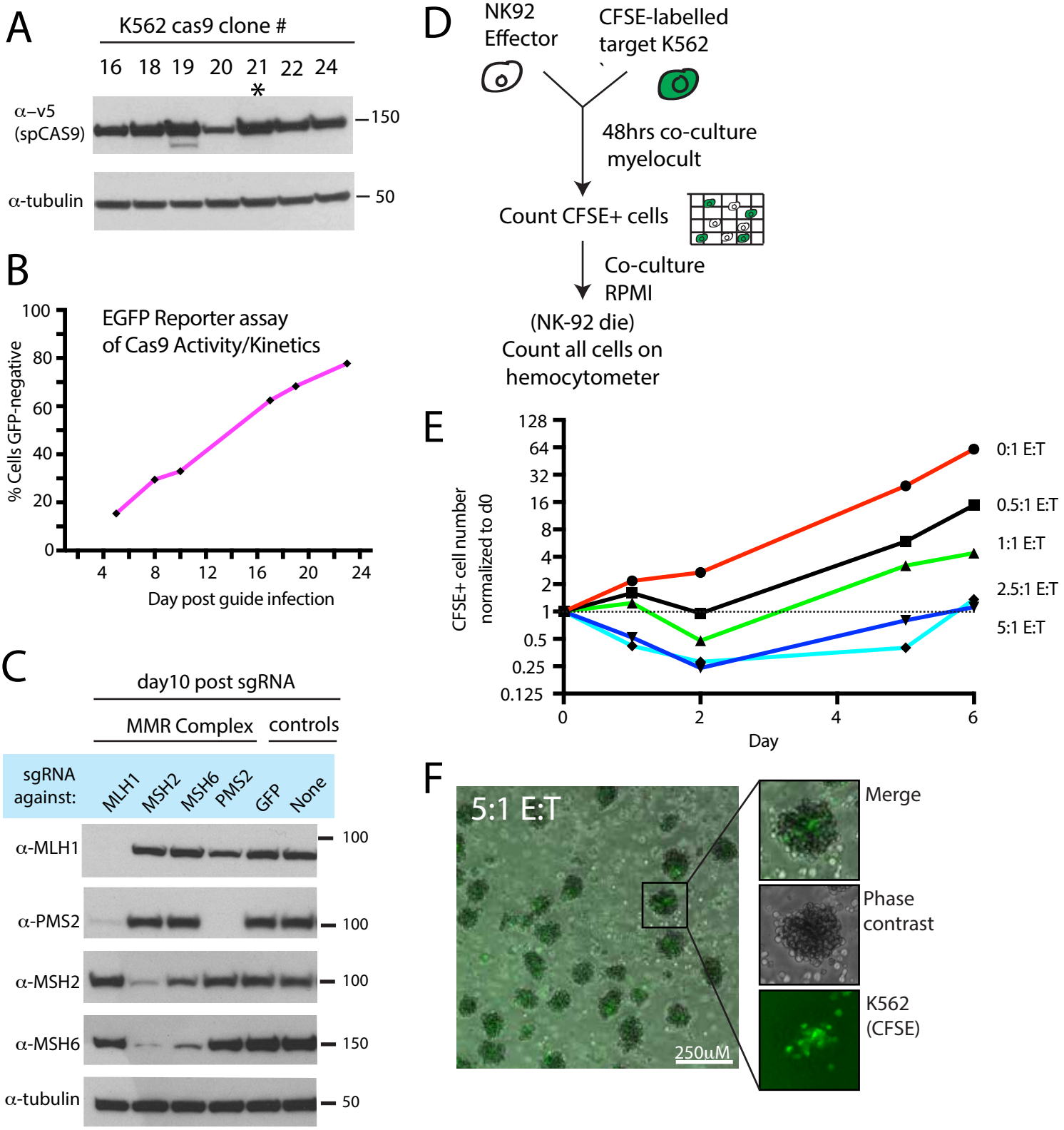
A
K562 cas9 clone #
16 18 19 20 21 22 24
*
α–v5 (spCAS9)
150
α-tubulin
50
B
EGFP Reporter assay of Cas9 Activity/Kinetics
% Cells GFP-negative
Day post guide infection
C
day10 post sgRNA
MMR Complex
controls
sgRNA against:
MLH1
MSH2
MSH6
PMS2
GFP
None
α-MLH1
α-PMS2
α-MSH2
α-MSH6
α-tubulin
D
NK92 Effector
CFSE-labelled target K562
48hrs co-culture myelocult
Count CFSE+ cells
Co-culture RPMI
(NK-92 die)
Count all cells on hemocytometer
E
CFSE+ cell number normalized to d0
Day
0:1 E:T
0.5:1 E:T
1:1 E:T
2.5:1 E:T
5:1 E:T
F
5:1 E:T
250μM
Merge
Phase contrast
K562 (CFSE)

Fig. S1

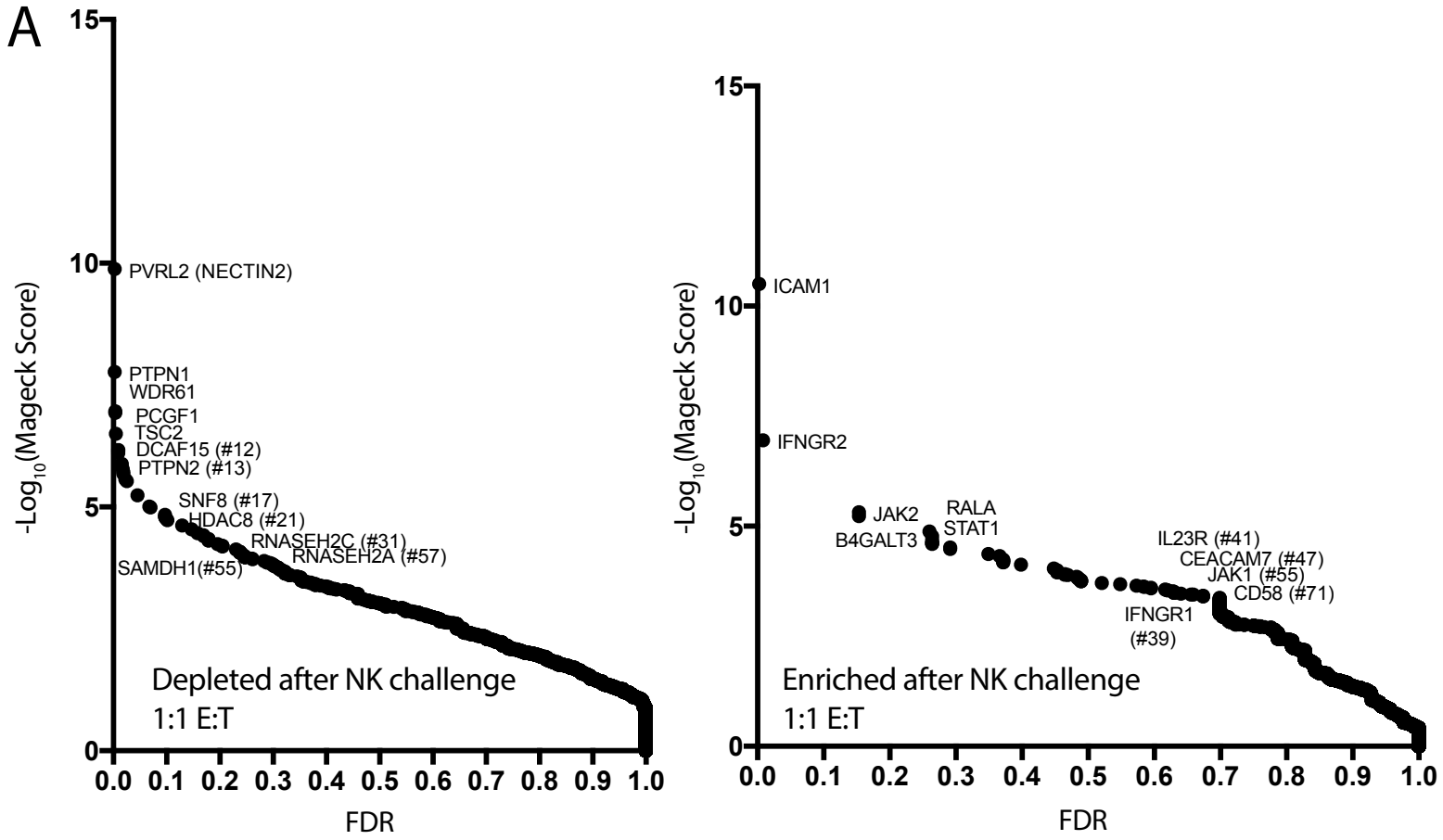
A
-Log10(Mageck Score)
FDR
PVRL2 (NECTIN2)
PTPN1
WDR61
PCGF1
TSC2
DCAF15 (#12)
PTPN2 (#13)
SNF8 (#17)
HDAC8 (#21)
RNASEH2C (#31)
RNASEH2A (#57)
SAMDH1(#55)
Depleted after NK challenge
1:1 E:T
ICAM1
IFNGR2
JAK2
RALA
STAT1
B4GALT3
IL23R (#41)
CEACAM7 (#47)
JAK1 (#55)
CD58 (#71)
IFNGR1
(#39)
Enriched after NK challenge
1:1 E:T

Fig. S2

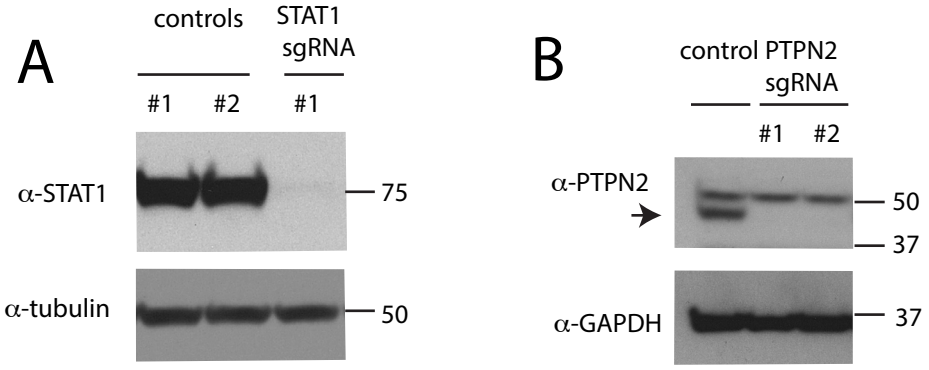
A
controls
STAT1 sgRNA
#1
#2
#1
α-STAT1
75
α-tubulin
50
B
control
PTPN2 sgRNA
#1
#2
α-PTPN2
50
37
α-GAPDH
37

Fig. S3

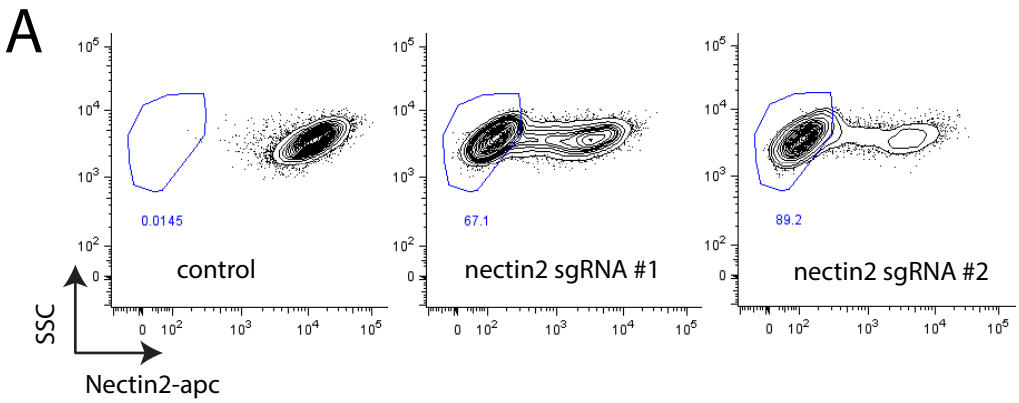
A
0.0145
control
67.1
nectin2 sgRNA #1
89.2
nectin2 sgRNA #2
SSC
Nectin2-apc

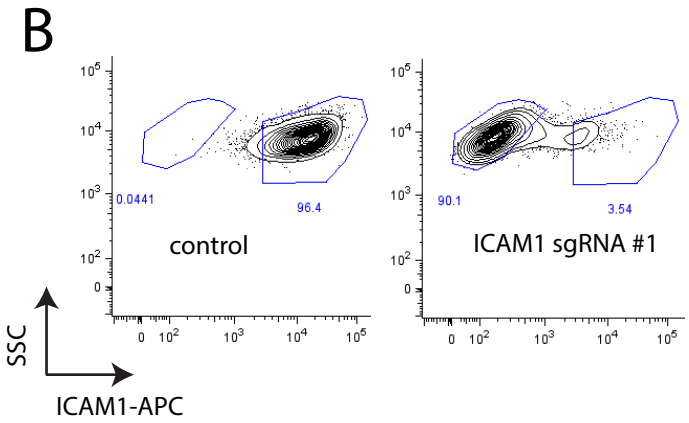
B
0.0441
96.4
control
90.1
3.54
ICAM1 sgRNA #1
SSC
ICAM1-APC

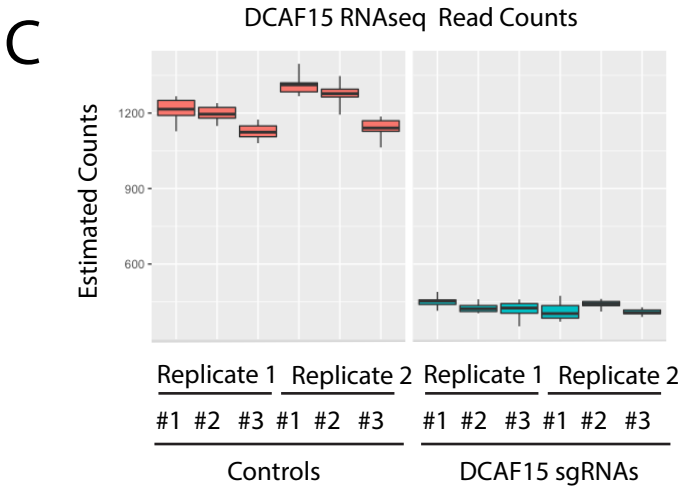
C
DCAF15 RNAseq Read Counts
Estimated Counts
1200
900
600
Replicate 1
Replicate 2
Replicate 1
Replicate 2
#1 #2 #3 #1 #2 #3
#1 #2 #3 #1 #2 #3
Controls
DCAF15 sgRNAs

Fig. S4

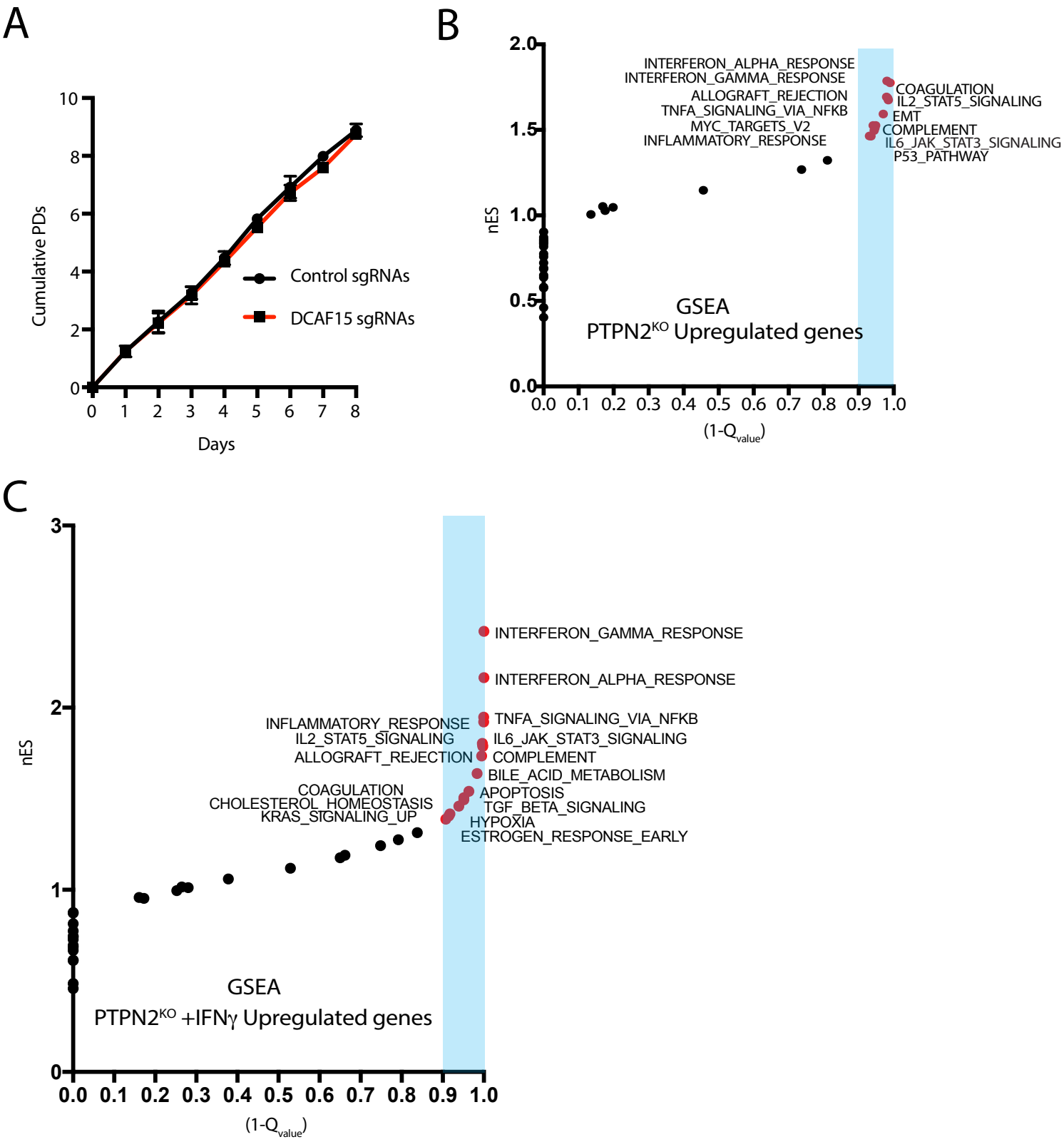
A
Cumulative PDs
Days
Control sgRNAs
DCAF15 sgRNAs
B
nES
(1-Q_value)
GSEA
PTPN2^KO Upregulated genes
INTERFERON_ALPHA_RESPONSE
INTERFERON_GAMMA_RESPONSE
ALLOGRAFT_REJECTION
TNFA_SIGNALING_VIA_NFKB
MYC_TARGETS_V2
INFLAMMATORY_RESPONSE
COAGULATION
IL2_STAT5_SIGNALING
EMT
COMPLEMENT
IL6_JAK_STAT3_SIGNALING
P53_PATHWAY
C
nES
(1-Q_value)
GSEA
PTPN2^KO +IFNγ Upregulated genes
INTERFERON_GAMMA_RESPONSE
INTERFERON_ALPHA_RESPONSE
TNFA_SIGNALING_VIA_NFKB
IL6_JAK_STAT3_SIGNALING
COMPLEMENT
BILE_ACID_METABOLISM
APOPTOSIS
TGF_BETA_SIGNALING
HYPOXIA
ESTROGEN_RESPONSE_EARLY
INFLAMMATORY_RESPONSE
IL2_STAT5_SIGNALING
ALLOGRAFT_REJECTION
COAGULATION
CHOLESTEROL_HOMEOSTASIS
KRAS_SIGNALING_UP

Fig. S5

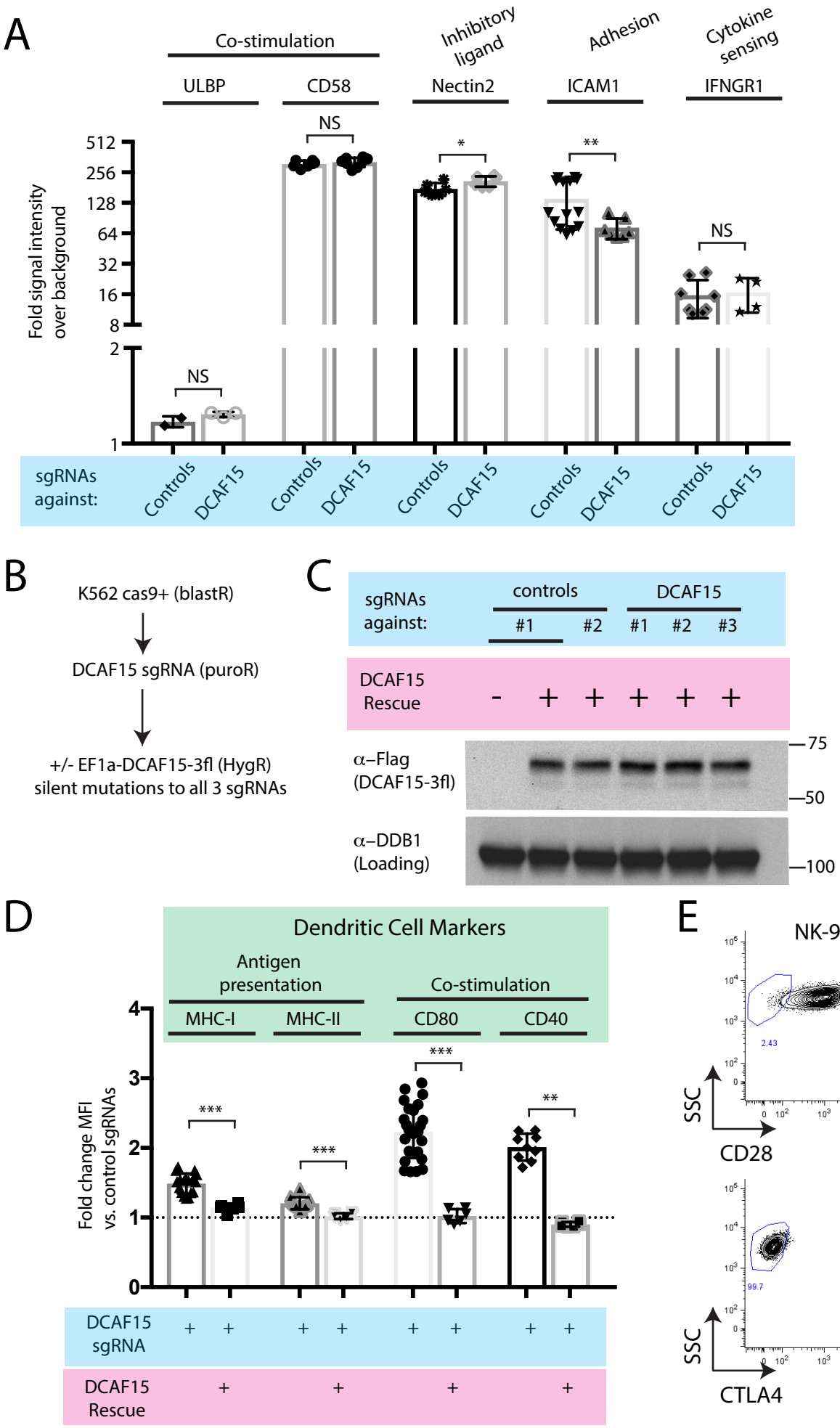
A
Co-stimulation
Inhibitory ligand
Adhesion
Cytokine sensing
ULBP
CD58
Nectin2
ICAM1
IFNGR1
Fold signal intensity over background
512
256
128
64
32
16
8
2
1
NS
*
**
NS
NS
sgRNAs against:
Controls
DCAF15
B
K562 cas9+ (blastR)
DCAF15 sgRNA (puroR)
+/- EF1a-DCAF15-3fl (HygR)
silent mutations to all 3 sgRNAs
C
sgRNAs against:
controls
DCAF15
#1
#2
#1
#2
#3
DCAF15 Rescue
-
+
+
+
+
+
α–Flag (DCAF15-3fl)
α–DDB1 (Loading)
75
50
100
D
Dendritic Cell Markers
Antigen presentation
Co-stimulation
MHC-I
MHC-II
CD80
CD40
Fold change MFI vs. control sgRNAs
4
3
2
1
0
***
***
***
**
DCAF15 sgRNA
DCAF15 Rescue
E
NK-92
2.43
SSC
CD28
99.7
SSC
CTLA4

Fig. S6

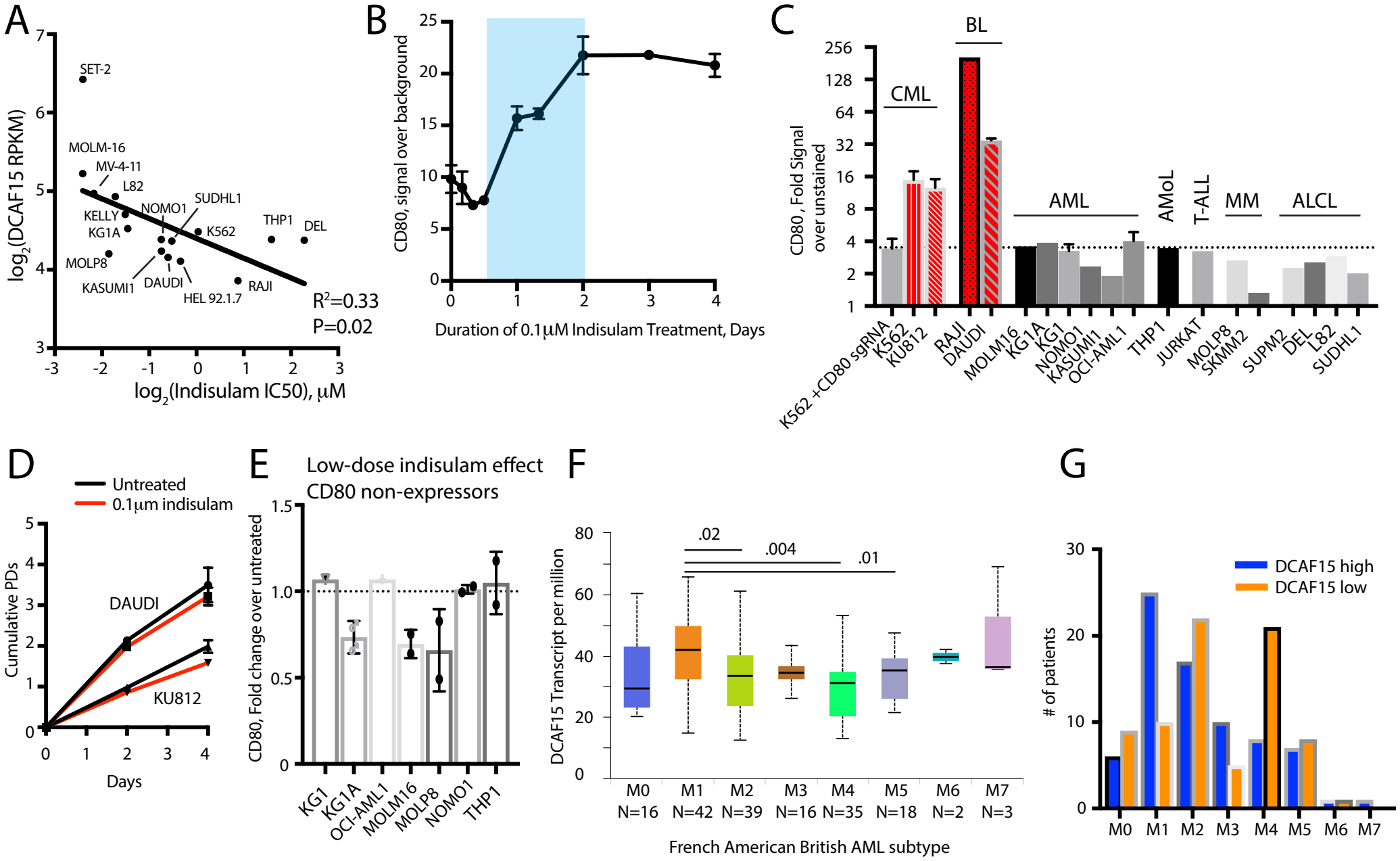
A
log2(DCAF15 RPKM)
log2(Indisulam IC50), μM
SET-2
MOLM-16
MV-4-11
L82
KELLY
KG1A
NOMO1
SUDHL1
K562
THP1
DEL
MOLP8
KASUMI1
DAUDI
HEL 92.1.7
RAJI
R2=0.33
P=0.02
B
CD80, signal over background
Duration of 0.1μM Indisulam Treatment, Days
C
CD80 , Fold Signal over unstained
CML
BL
AML
AMoL
T-ALL
MM
ALCL
K562 +CD80 sgRNA
K562
KU812
RAJI
DAUDI
MOLM16
KG1A
KG1
NOMO1
KASUMI1
OCI-AML1
THP1
JURKAT
MOLP8
SKMM2
SUPM2
DEL
L82
SUDHL1
D
Untreated
0.1μm indisulam
Cumulative PDs
DAUDI
KU812
Days
E
Low-dose indisulam effect
CD80 non-expressors
CD80, Fold change over untreated
KG1
KG1A
OCI-AML1
MOLM16
MOLP8
NOMO1
THP1
F
DCAF15 Transcript per million
.02
.004
.01
M0 N=16
M1 N=42
M2 N=39
M3 N=16
M4 N=35
M5 N=18
M6 N=2
M7 N=3
French American British AML subtype
G
DCAF15 high
DCAF15 low
# of patients
M0
M1
M2
M3
M4
M5
M6
M7

Fig. S7

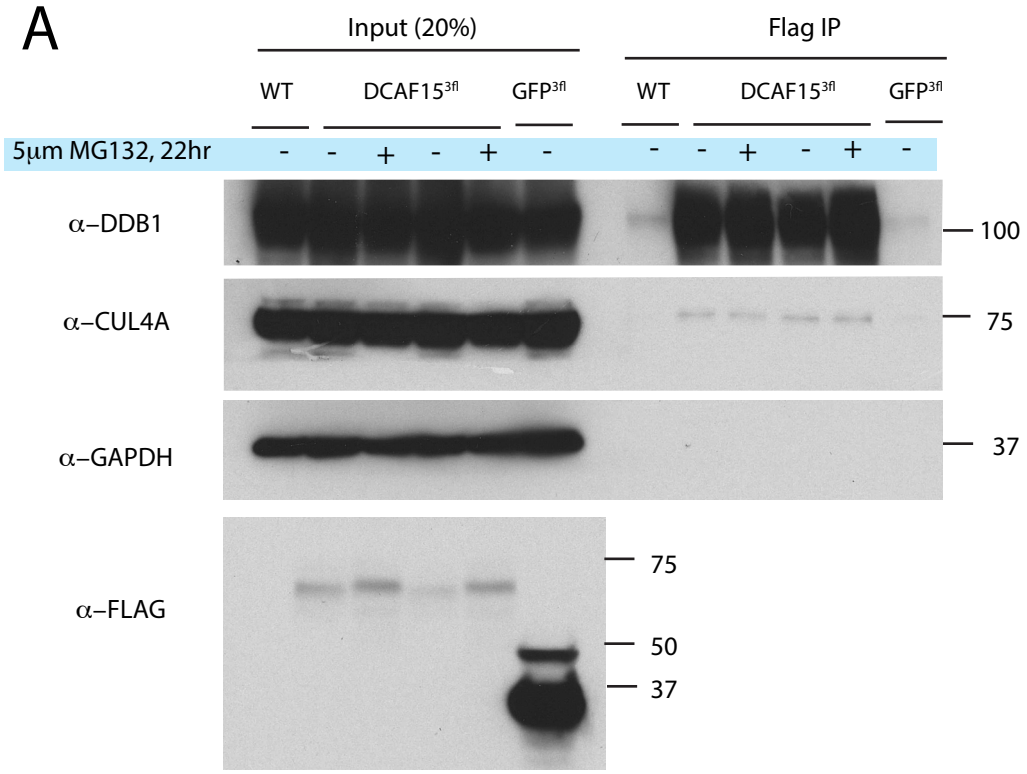
A
Input (20%)
Flag IP
WT
DCAF15^{3fl}
GFP^{3fl}
WT
DCAF15^{3fl}
GFP^{3fl}
5μm MG132, 22hr
- - + - + -
- - + - + -
α–DDB1
100
α–CUL4A
75
α–GAPDH
37
α–FLAG
75
50
37

Fig. S8